EUROPEAN COMMISSION
5th EURATOM FRAMEWORK PROGRAMME 1998-2002
KEY ACTION : NUCLEAR FISSION

HTR-E

High-Temperature Reactor Components and Systems

CONTRACT N°
FIKI-CT-2001-00177

WP1

Helium Turbine Design Study

Deliverable n°7a

Jean-François Brouckaert,
René Van den Braembussche

von Karman Institute

Belgium

Dissemination level : RE
Document N°: HTR-E 03/12 D-1-1-5-1
Status : Preliminary
Deliverable n°7a

von Karman Institute for Fluid Dynamics INPA
Chaussée de Waterloo, 72
B-1640 RHODE-SAINT-GENESE, BELGIUM.

CONTRACT N°
FIKI-CT-2001-00177

WP1

Helium Turbine Design Study

Deliverable n°7a

Jean-François Brouckaert,
René Van den Braembussche

von Karman Institute

Belgium

7

HTR-E WP1

-

PART I - HELIUM TURBINE DESIGN

1. Design Conditions.

The design conditions for the turbine are shown in Table 1.

Working Gas	Helium
Type	Horizontal axial flow
Rotational Speed	3000 RPM
Mass Flow Rate	316 kg/s
Inlet Temperature	1121.2 K
Outlet Temperature	783.2 K
Inlet Pressure	70.1 bar
Outlet Pressure	26.4 bar
Pressure Ratio	2.65

Table 1. Design conditions for the turbine.

2. Choice of the Operating Point : General Considerations.

Before the aerodynamic design can be carried out, some general considerations must be looked at in terms of number of stages and loading per stage, overall geometry of the turbine and targeted efficiency.

For this purpose, Smith's diagram was used (Figure 1.) which relates the stage loading factor Ψ to the stage flow factor Φ in an efficiency map. The efficiency curves shown in Smith's diagram were obtained for different families of turbine stages for gas turbines at zero tip leakage. As it can be seen, reducing the stage loading and the flow factor improves the stage efficiency. Reducing the stage loading requires more stages for a given diameter or requires to work at higher diameters and thus higher peripheral speeds, which means also a higher stress level for the disk. On the other hand, for a given mass flow rate and peripheral speed, if the flow factor is reduced, the blade height will increase which improves the efficiency but causes also higher stresses at the blade root.

It was therefore decided to investigate the various parameters playing an important role into the aerodynamic and mechanical design of the machine. This parametric study was carried out along the line drawn in Smith's diagram, which was chosen as the "maximum loading" line. Indeed, for each efficiency curve, there exists a point for which the stage loading Ψ is maximum, which will result in the smallest possible number of stages for the given work to be performed at that targeted efficiency. The corresponding value of the flow factor Φ and hence the blade height is a consequence of the stage loading at that efficiency.

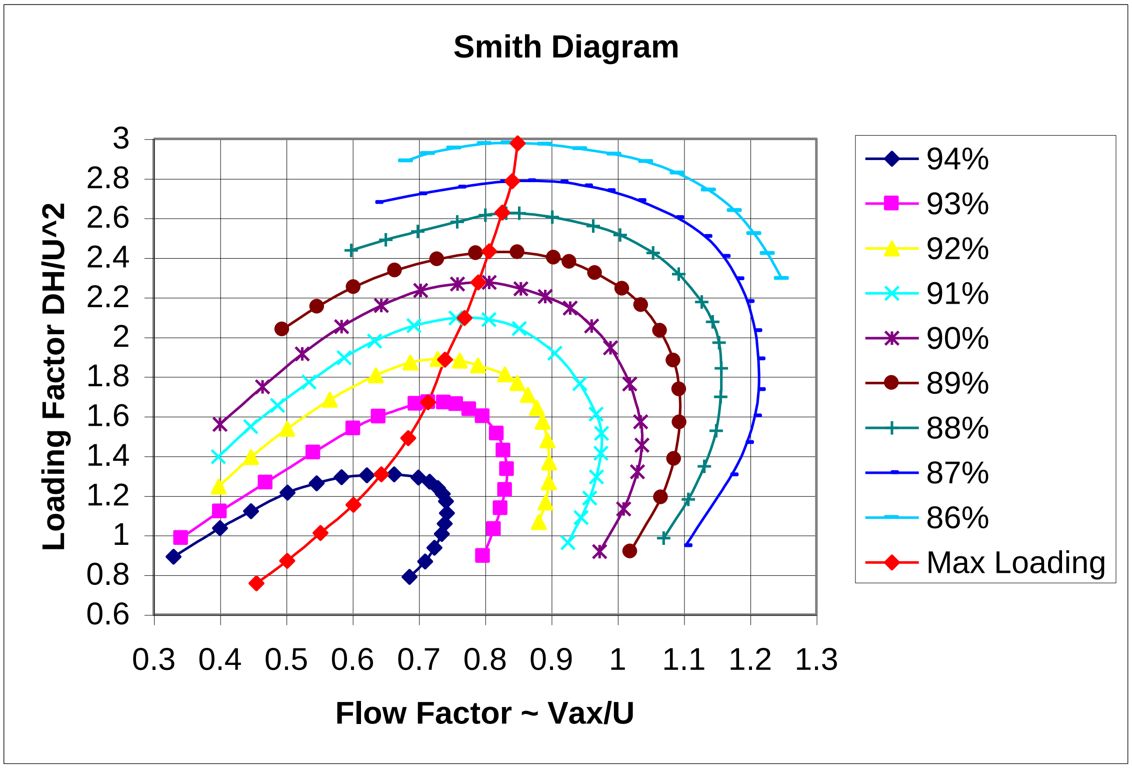

Figure 1. Smith's diagram : turbine stage efficiency at zero tip leakage.

Each point of the maximum loading line corresponds to a couple (Ψmax, Φ) and will be referenced in the following graphs by its corresponding efficiency. Each loading factor Ψmax can be obtained for different number of stages at different peripheral speeds as shown in the following equation and presented in Figure 2.

$$\Psi = \frac{\Delta Hstage}{U^2} = \frac{\Delta Htotal}{Nstages} \frac{1}{U^2}$$

This means that if the design is constrained by a maximum number of stages, the choice of a targeted efficiency will determine the peripheral speed U required to do the work. At a fixed rotational speed (3000 RPM), this directly fixes the radius of the turbine disk as shown in Figure 3. On the other hand, if a maximum diameter is imposed for the turbine disk, then the peripheral speed U is fixed, and the number of stages will be determined by the targeted efficiency.

On the other hand, considering the flow coefficient Φ corresponding to the "maximum loading" line, we have on the different efficiency lines :

$$\Phi = \frac{Vax}{U}$$

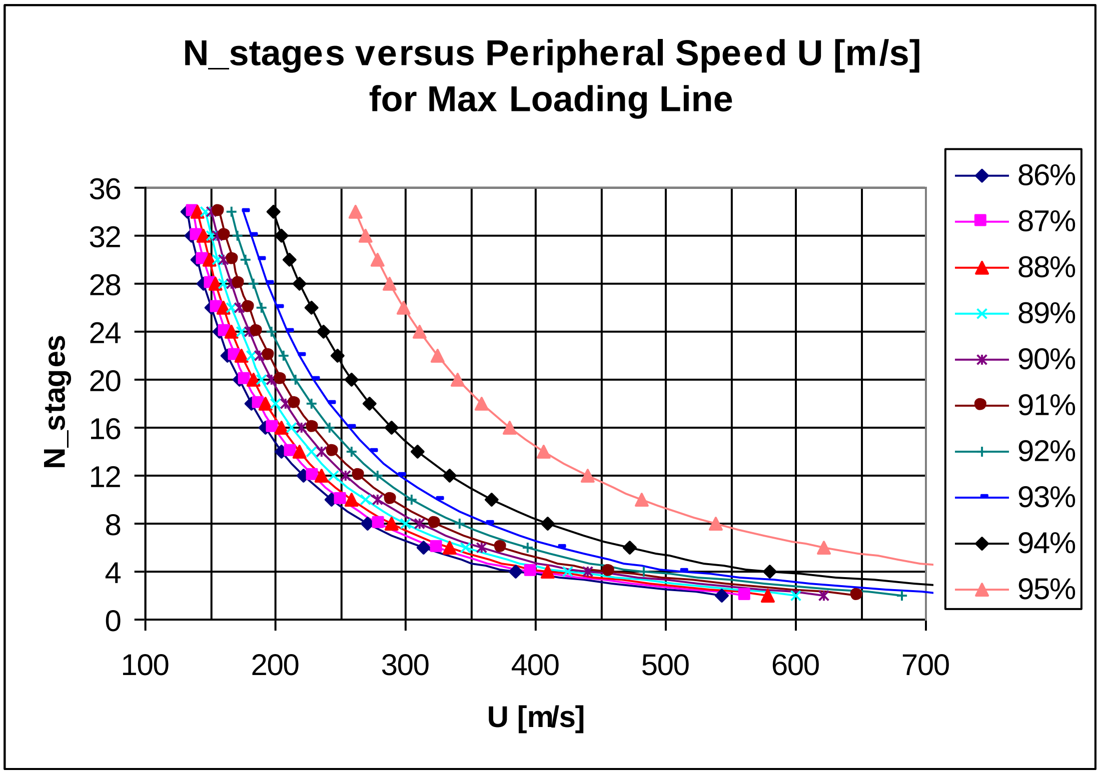

Figure 2. Number of stages versus peripheral speed U [m/s].

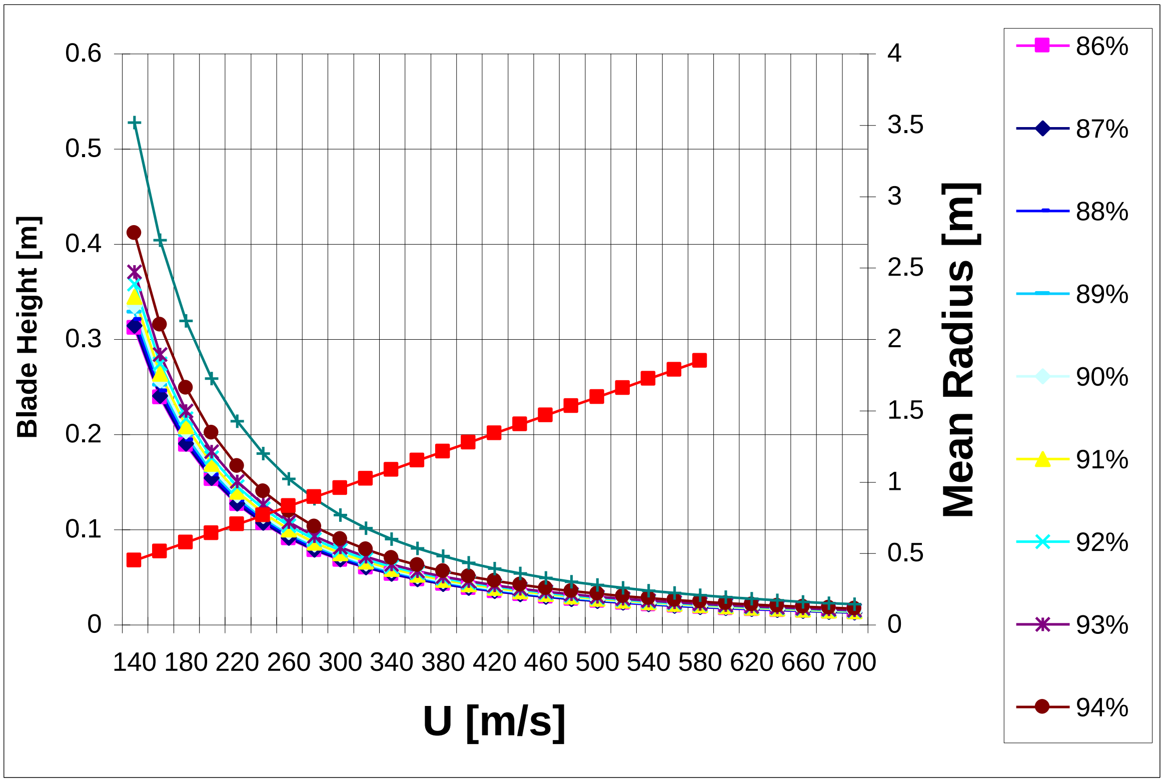

Figure 3. Blade Height and Mean radius as a function of peripheral speed at 3000 RPM.

It can be shown that the blade height in inversely proportional to the flow coefficient Φ :

$$H = \frac{\dot{m}\omega}{2\pi\rho\Phi U^2}$$

For a given Φ corresponding to a given efficiency line in the Smith diagram, the blade height H will therefore decrease as the peripheral speed increases (see Figure 3). If Φ increases at a given peripheral speed U, Vax will increase as well which leads in turn to a smaller blade height.

From an aerodynamic point of view, smaller blade heights will lead to more annulus losses and secondary flows occupy rapidly a more important portion of the flow passage, resulting in a rapid drop in efficiency (Figure 4.).

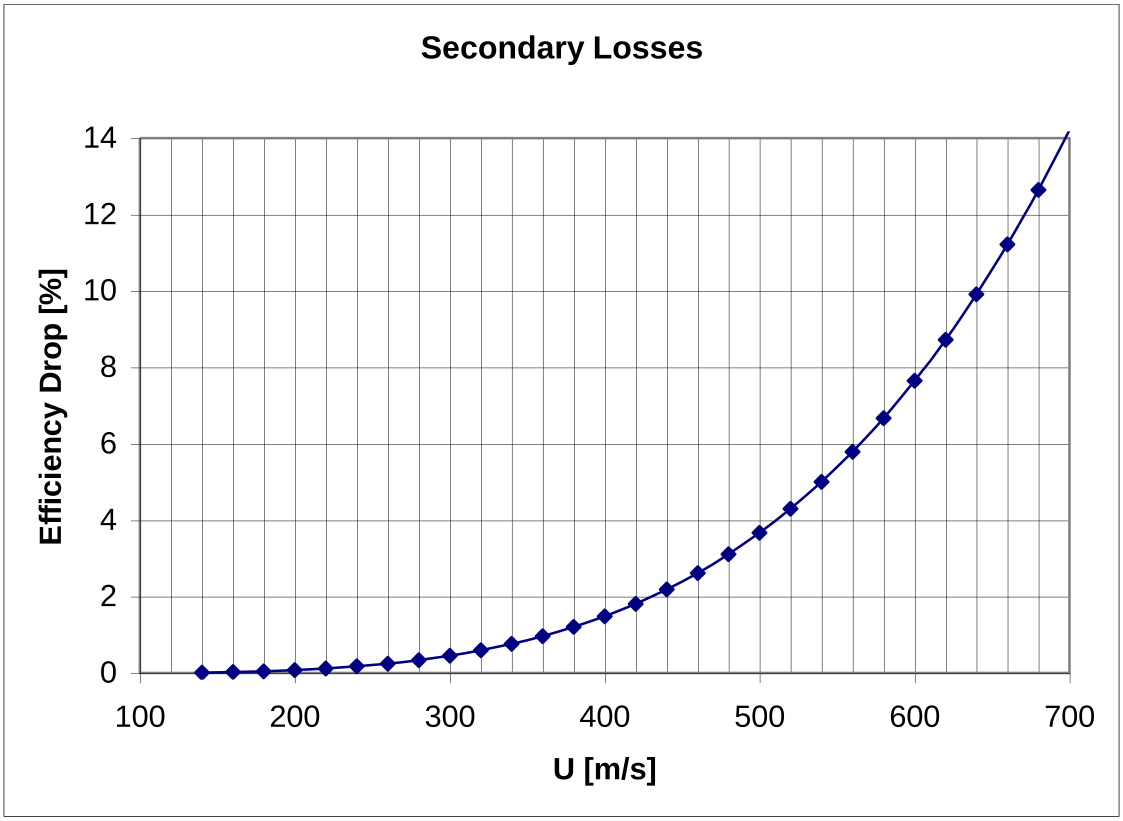

Figure 4. Efficiency Loss due to Secondary Flows as a function of peripheral speed.

Of course, from a mechanical point of view, smaller blade heights cause lower stresses at the blade root (Figure 5.) but as the mean radius of the machine increases at the same time, the stresses on the shaft are increasing as a result of larger rotor disks (Figure 6).

Obviously, among those various considerations, a compromise has to be made between the constraints set by the mechanical limits and those set by the aerodynamic performance requirements.

If we consider both the mechanical and aerodynamic limits by overlaying Figure 6 onto Figure 2, we obtain 2 sets of curves crossing eachother (Figure 7.).

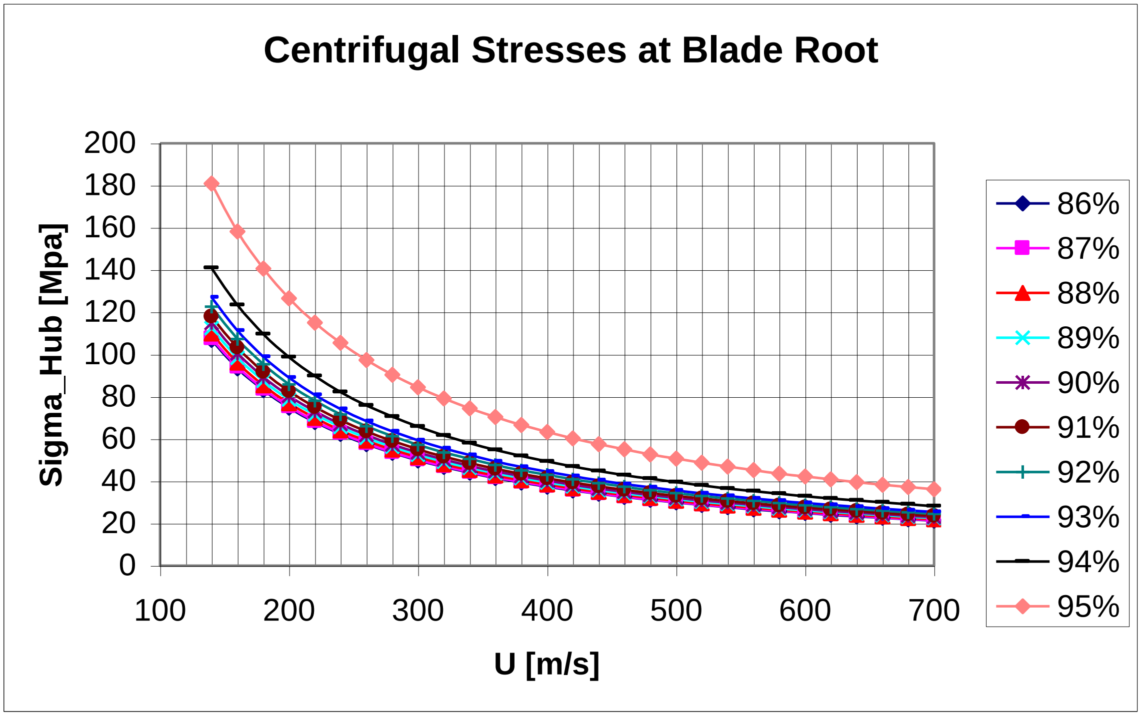

Figure 5. Centrifugal stresses at the blade root versus peripheral speed.

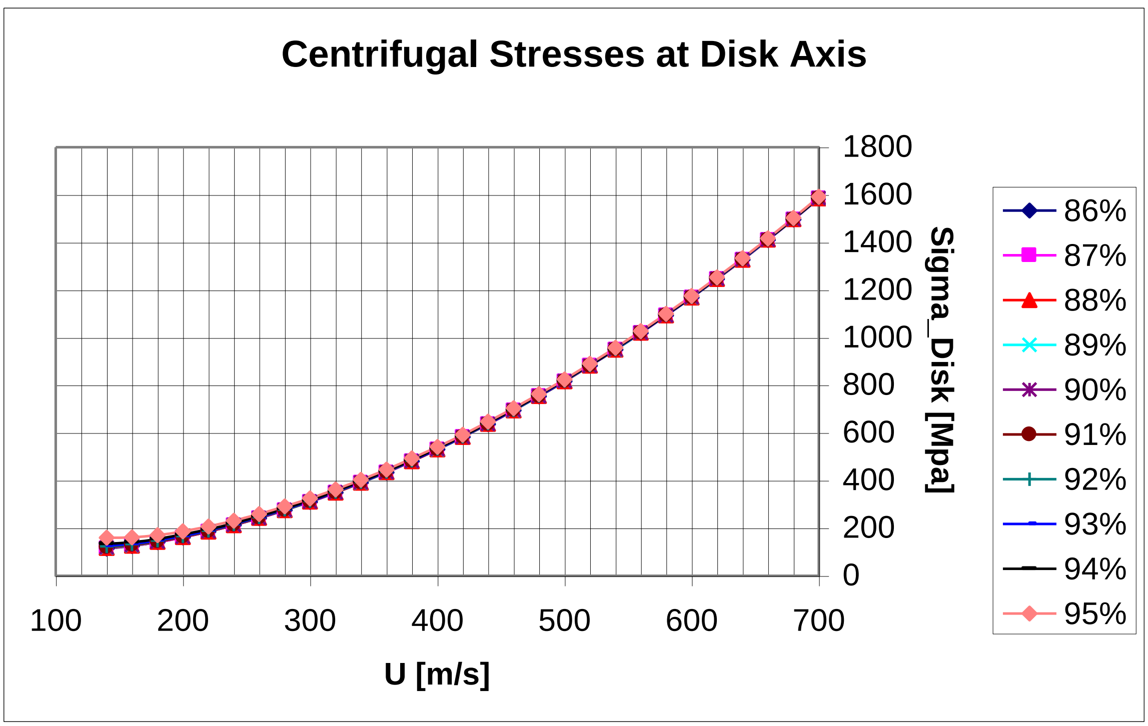

Figure 6. Centrifugal stresses at the blade root versus peripheral speed.

Several choices may be interesting. First, if we consider that no more than 12 turbine stages should be used, then to limit the mechanical stresses while keeping a good efficiency of 93%, we can choose the operating point Nr. 1 on the map, corresponding to a speed of 280 m/s. Geometrically, this choice is very similar to the Russian design of the GTMHR. Two other possibilities are indicated on the map by point Nr. 2 and Nr. 3. In the case where 12 stages are kept, increasing the tip speed to 350 m/s would lead to a gain of more than 1% in efficiency, i.e. 94% (point Nr. 2). If the stresses are acceptable at this peripheral speed, another possibility would be to reduce the number of stages to 8, keeping the same efficiency as for the 12-stage configuration (point Nr. 3).

At this point, it was decided to develop the design of point Nr. 1, which corresponds to the lowest stress level among the 3 possibilities that were pointed out.

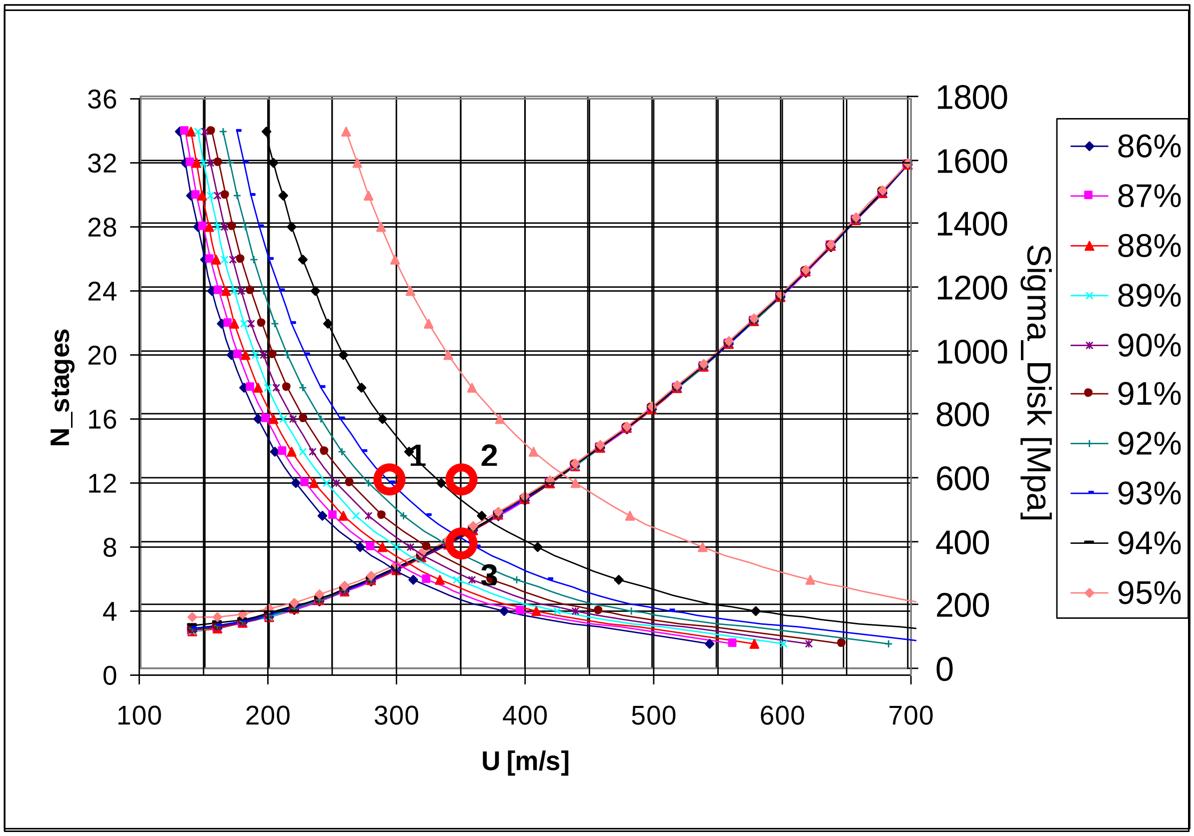

Figure 7. Combined chart of number of stages and centrifugal stresses at the turbine shaft versus peripheral speed.

3. <u>Through Flow Analysis – One-dimensional Design.</u>

The turbine overall performance is predicted by means of the VKI analysis program MAP (Meanline Analysis Program). This program predicts the flow variation from hub to shroud at all sections between stator and rotor. It is based on the equations of radial equilibrium and makes use of different turbine loss correlations.

The predictions discussed here are obtained with the correlations of Soderberg (De Michele, 1975, McDonald, 1975).

The detailed flow conditions are shown in Table 2 below for stages 1, 2, 11 and 12. The flow conditions are almost identical in all stages from stage 1 to 11 with a degree of reaction r = 0.3. The last stage operates with a lower degree of reaction, r = 0.19 to obtain a nearly axial outlet flow. The shaft power, not taking into account the mechanical losses and inlet/outlet duct losses is 569.58 MW. The corresponding total-to-total and total-to-static efficiencies for the whole machine are respectively η_{TT}=93.38% and η_{TS}=92.32%.

	Stage 1	**Stage2**	**Stage 11**	**Stage 12**
	STATOR			
$\alpha_{1stator}$ [deg.]	0.0	-30.29	-24.37	-23.49
$\alpha_{2stator}$ [deg.]	68.98	69.00	65.89	64.28
θ_{stator} [deg.]	68.98	99.29	90.26	87.77
$Ma_{abs,stator}$ [-]	0.260	0.264	0.309	0.304
σ_{stator} [-]	1.051	1.068	1.062	1.054
$N_{blades,stator}$	51	60	65	67
	ROTOR			
β_{1rotor} [deg.]	49.20	49.22	43.58	39.48
β_{2rotor} [deg.]	-63.95	-63.77	-59.91	-52.39
θ_{rotor} [deg.]	113.1	113.0	103.5	91.87
$Ma_{rel,rotor}$ [-]	0.21	0.213	0.252	0.214
σ_{rotor} [-]	1.264	1.265	1.264	1.267
$N_{blades,rotor}$	137	138	144	151
	STAGE			
Degree of Reaction	0.3	0.3	0.3	0.19
Ψ	2.19	2.18	2.07	1.67
Φ	0.68	0.68	0.77	0.78
Adiabatic eff. η_{TT}	0.9256	0.9144	0.9248	0.9284

Table 2. Results of Through Flow Calculations.

4. Two-dimensional Blade Design.

The two-dimensional design of the blade sections is done by means of an inverse design and optimization method. The latter uses an iterative approach that combines a direct solver with a blade geometry modification algorithm. A potential flow method was used in the present blade design. The procedure starts with the analysis of a given cascade geometry using the flow solver. The differences between the calculated and required velocity is used as an input for the modification algorithm based on a transpiration technique. This algorithm provides a new blade shape for which the calculated velocity distribution is closer to the desired one. A major advantage of this method is that the design cycle is very short and allows an easy off-design analysis since the same code is used for the blade design and the analysis for different inlet flow conditions.

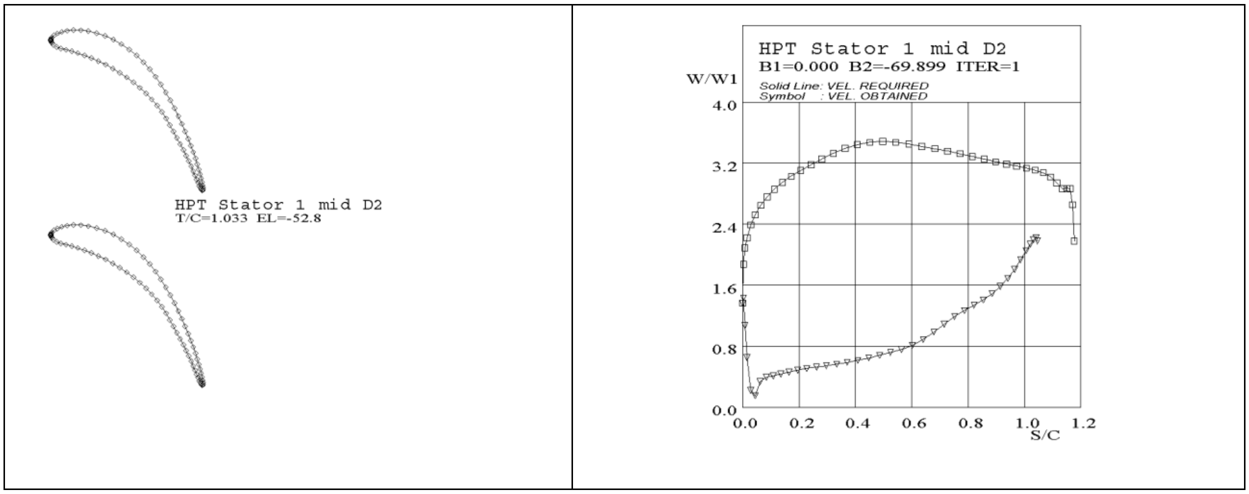

Figure 8. 2D Blade Section and Velocity Distribution for first stage HPT stator.

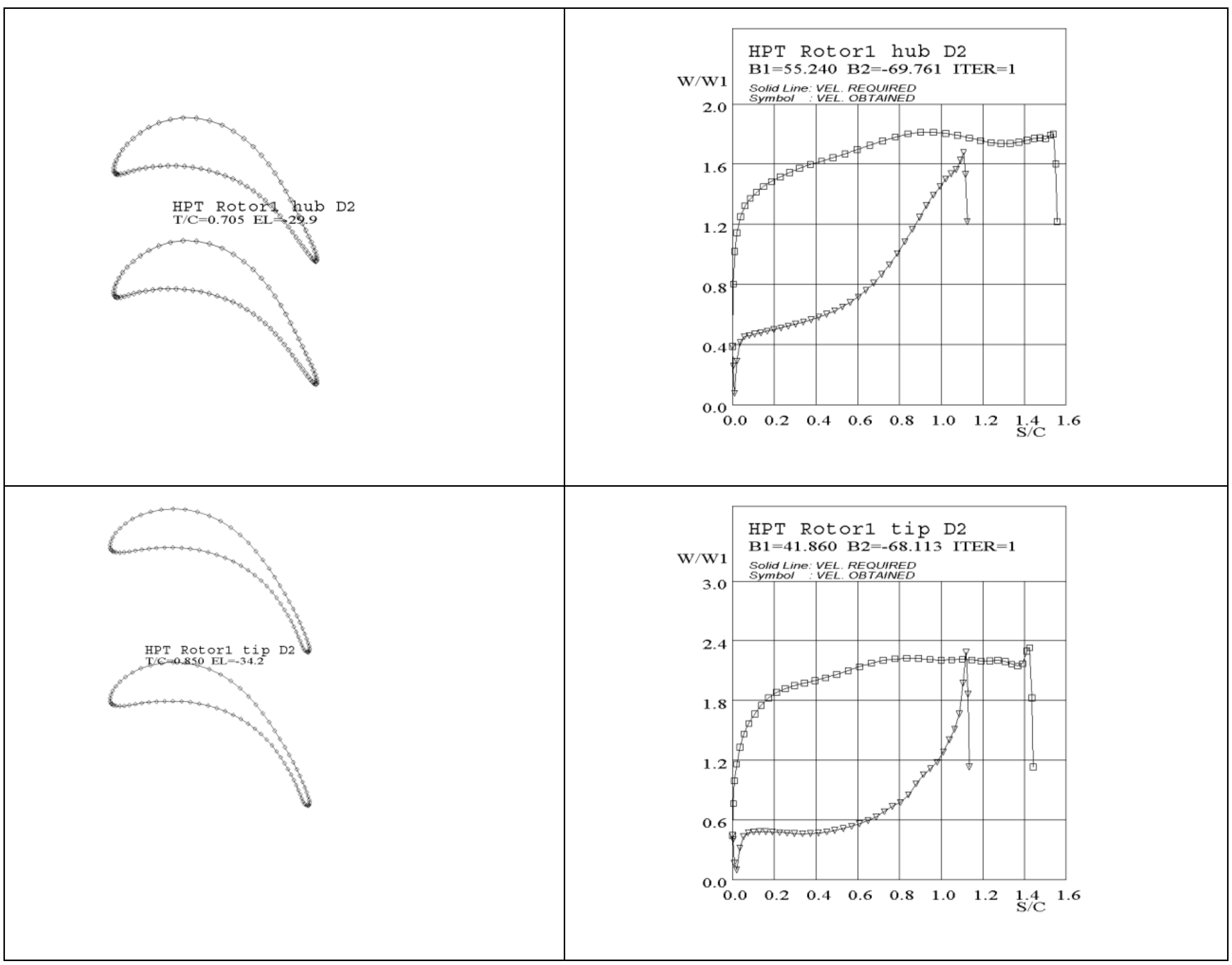

Figure 9. 2D Blade Hub and Tip Sections and Velocity Distributions for first stage HPT rotor.

The two-dimensional blade design results are presented in Figures 8, 9, and 10 respectively for the first-stage stator blade, for the first-stage rotor blade and for the second-stage stator blade. Since the outlet flow angle distributions are approximately constant over the blade height, cylindrical stators have been designed on the basis of the flow conditions at midspan.

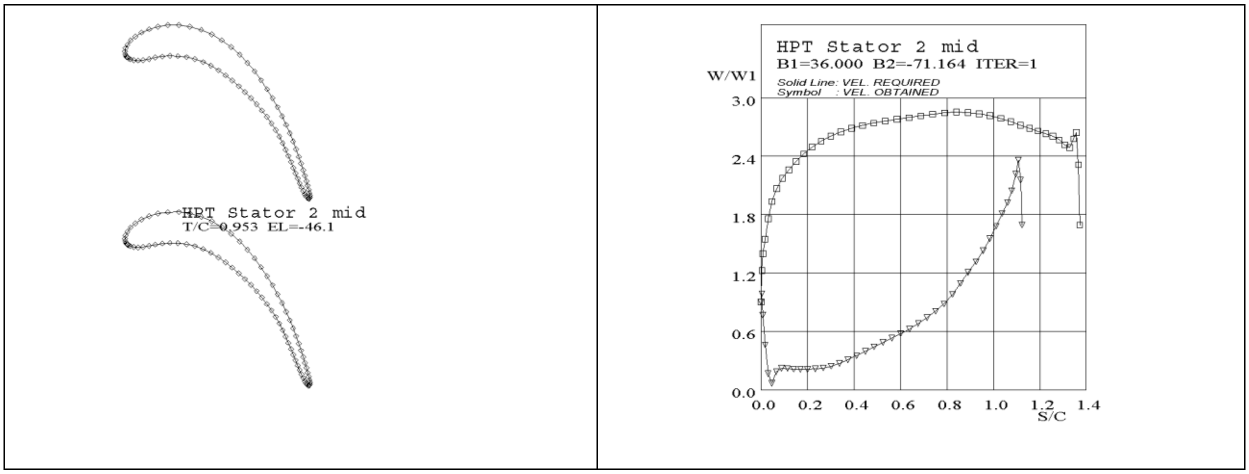

Figure 10. 2D Blade Section and Velocity Distribution for second stage HPT stator.

5. <u>Three-dimensional Navier-Stokes analysis.</u>

Since the two-dimensional blade design is performed with an inviscid method, the blade rows need to be analyzed by means of a Navier-Stokes solver to assess its viscous performance with respect to the one-dimensional through flow design.

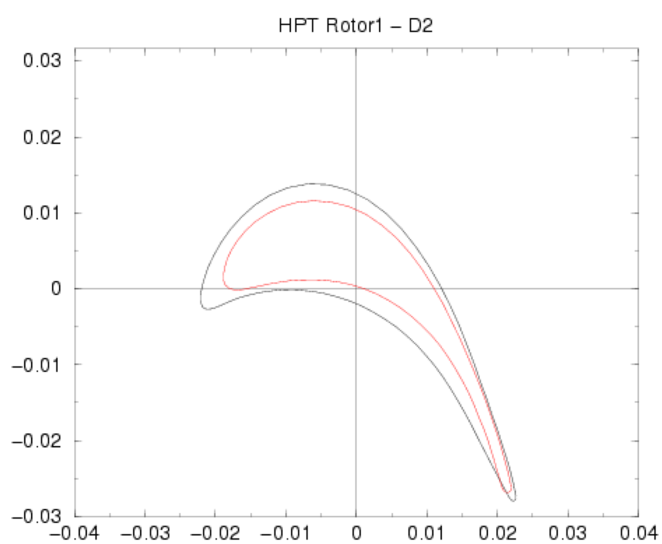

Figure 11. HPT Rotor 3D blade staking along CG.

Figure 11 shows the 3D blade stacking of the rotor along the center of gravity of each section. Figure 12 shows a top view of the first two stages with their respective blade counts as they have been designed and analyzed with the Navier-Stokes solver. A first set of calculations was performed on stage 1 and a second set on stage 2 in which rotor 1 was used behind stator 2.

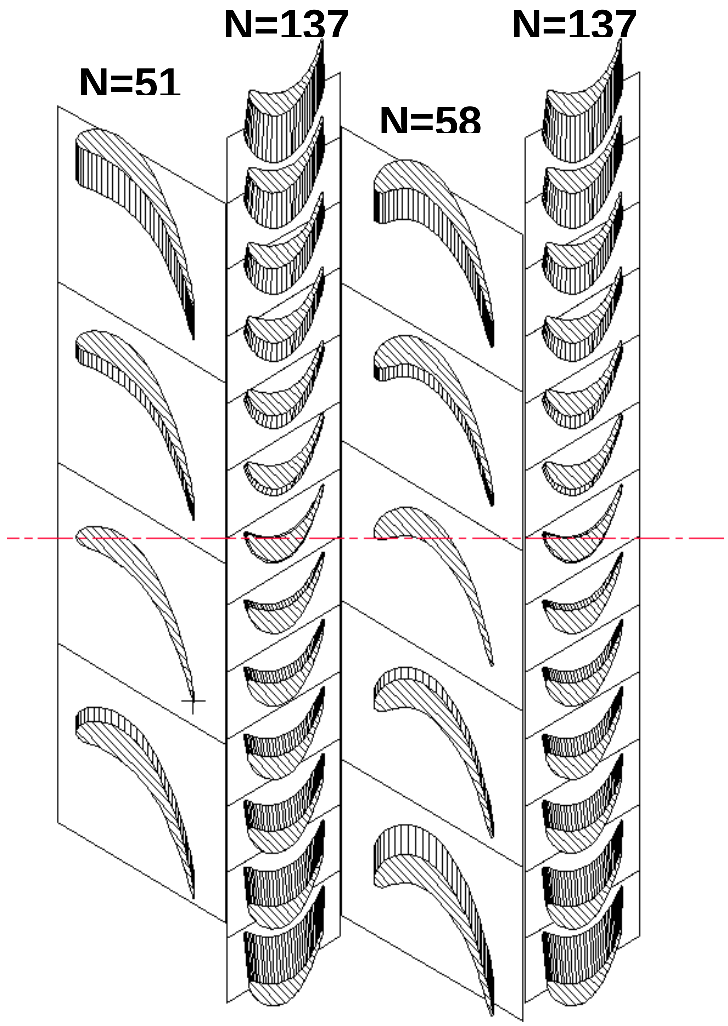

Figure 12. Top view of the 3D geometry of the first two stages.

The isentropic Mach number distributions are shown in Figure 13 for stator 1 and rotor 1 respectively at 10%, 50%, and 90% blade height. Both sets of distributions show a smooth acceleration until 65-70% of the axial chord and then a slight deceleration. Figure 14 shows the outlet angle distributions for stage 1. Figure 15 shows the radial distributions of total and static pressures and Figure 16 shows the radial distributions of isentropic Mach number and degree of reaction. After Navier-Stokes computations, the total-to-total stage efficiency obtained is 93.63% with a pressure ratio of 0.9305.

The corresponding data for stage 2 are presented in Figure 17, 18, and 19.

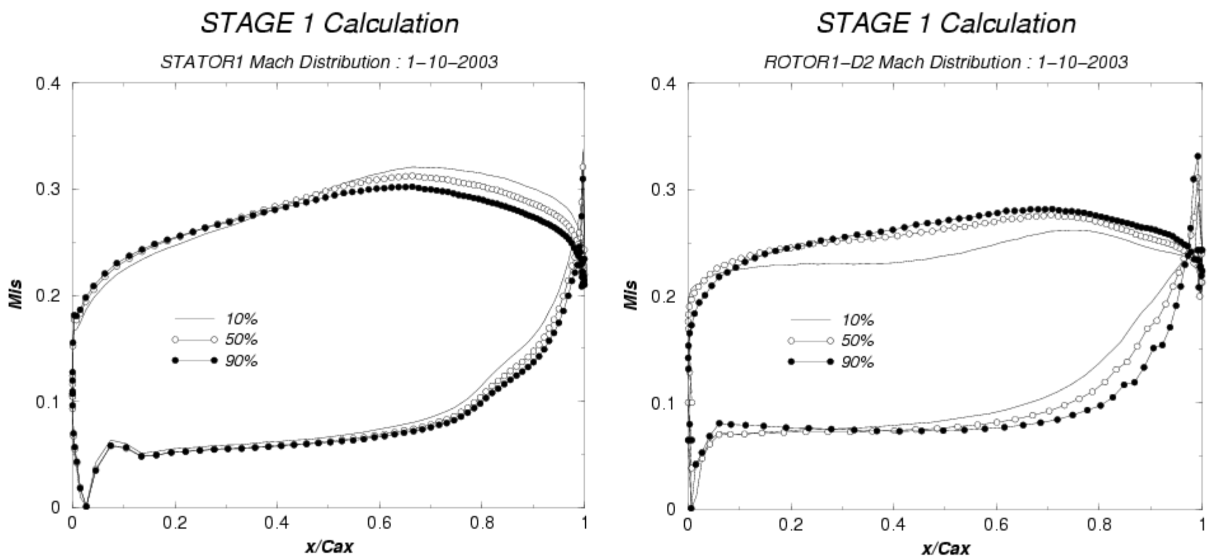

Figure 13. Isentropic Mach Number distributions on HPT Stator1 and Rotor 1.

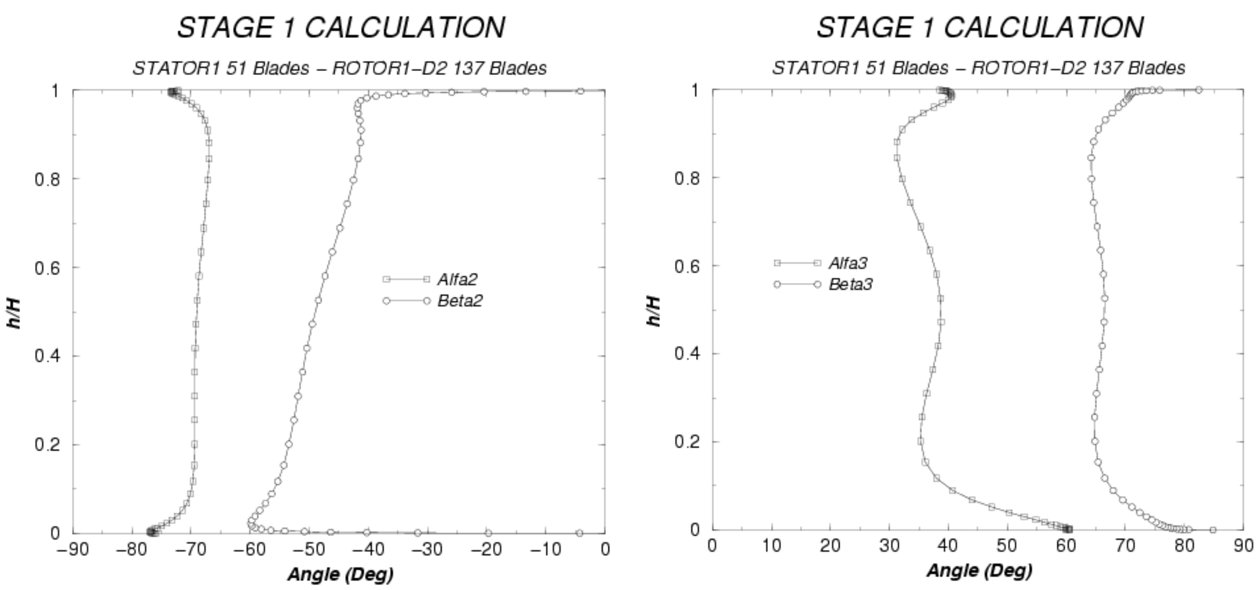

Figure 14. Absolute and relative outlet angle distributions for HPT Stator1 and Rotor 1.

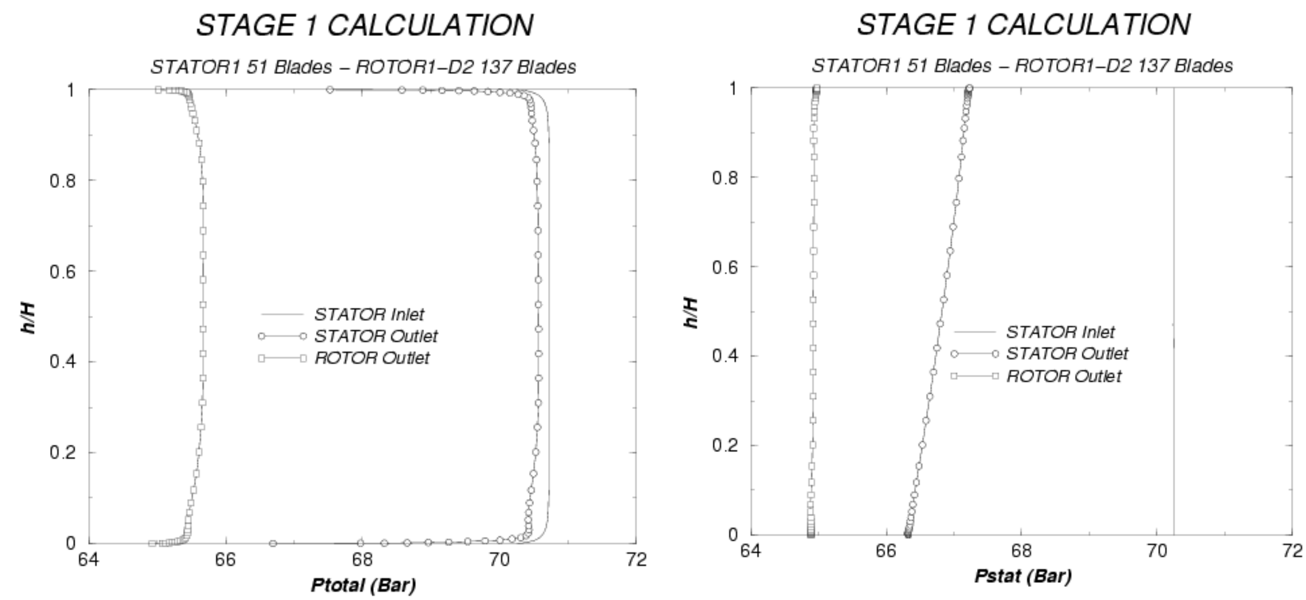

Figure 15. Total and Static pressure radial distributions for HPT Stator1 and Rotor 1.

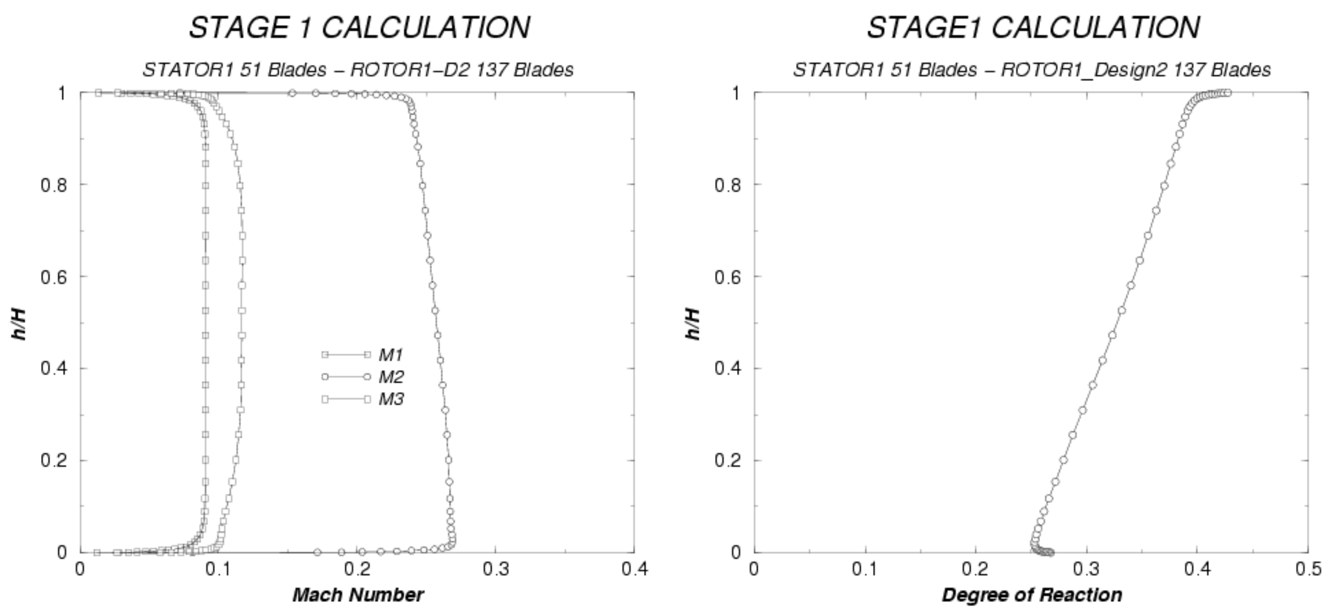

Figure 16. Isentropic Mach Number and Degree of Reaction radial distributions for HPT Stage 1.

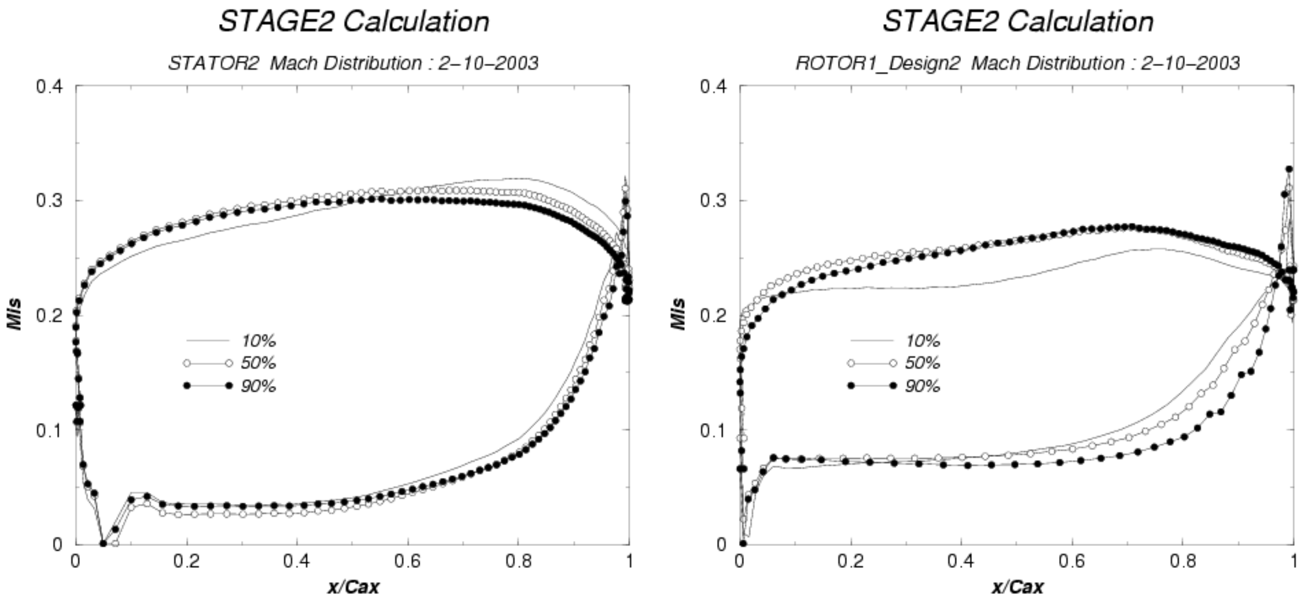

Figure 17. Isentropic Mach Number distributions on HPT Stator2 and Rotor 1.

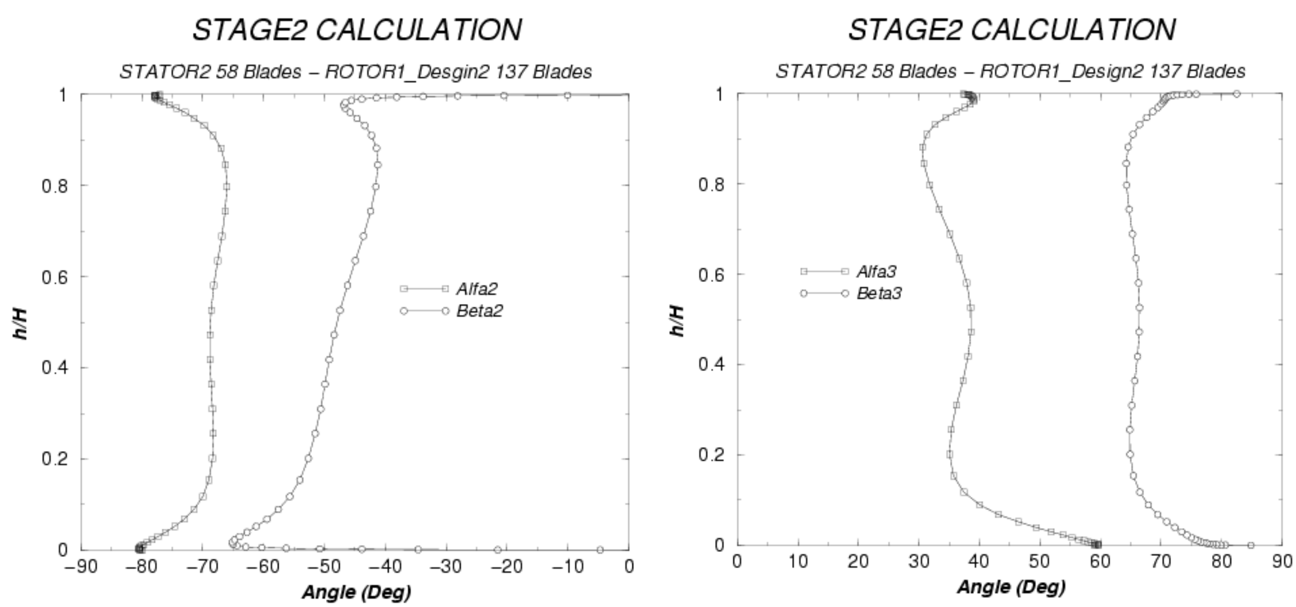

Figure 18. Absolute and relative outlet angle distributions for HPT Stator2 and Rotor 1.

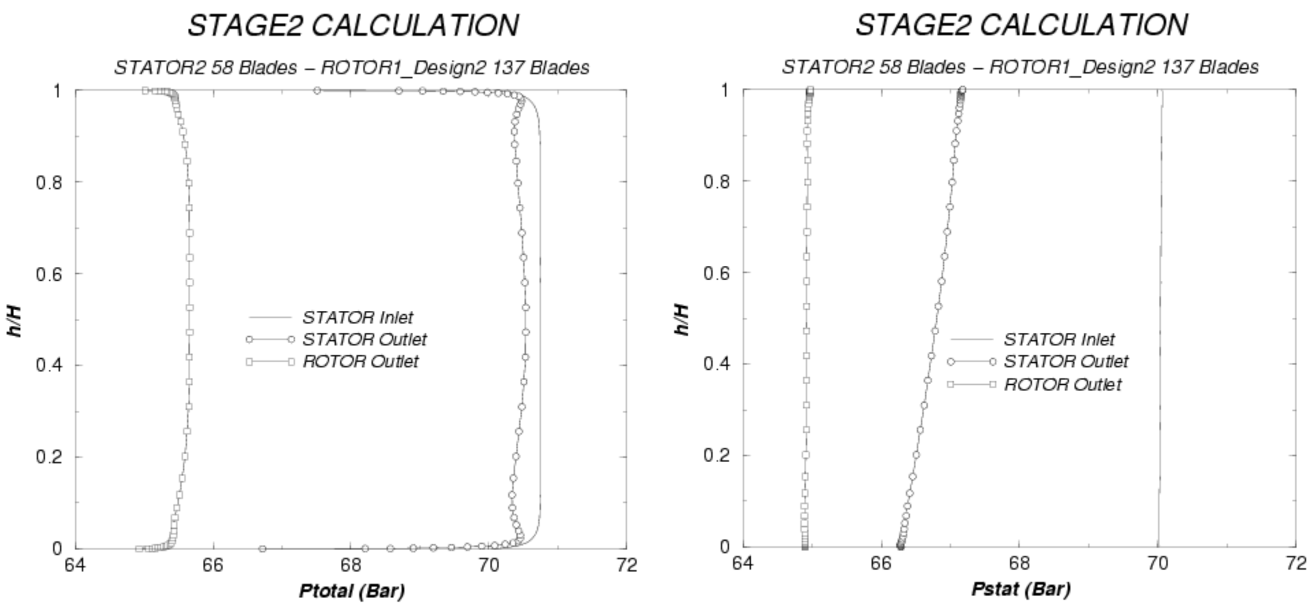

Figure 19. Total and Static pressure radial distributions for HPT Stator2 and Rotor 1.

6. <u>CAD design for Mechanical Analysis.</u>

A CAD design of both HPT stages was carried out in order to allow the geometry to be transmitted to the contract partner (Empresarios Agrupados) in charge of the mechanical analysis. The rotor root design is of the conventional "pine-three" type and the stator is shrouded.

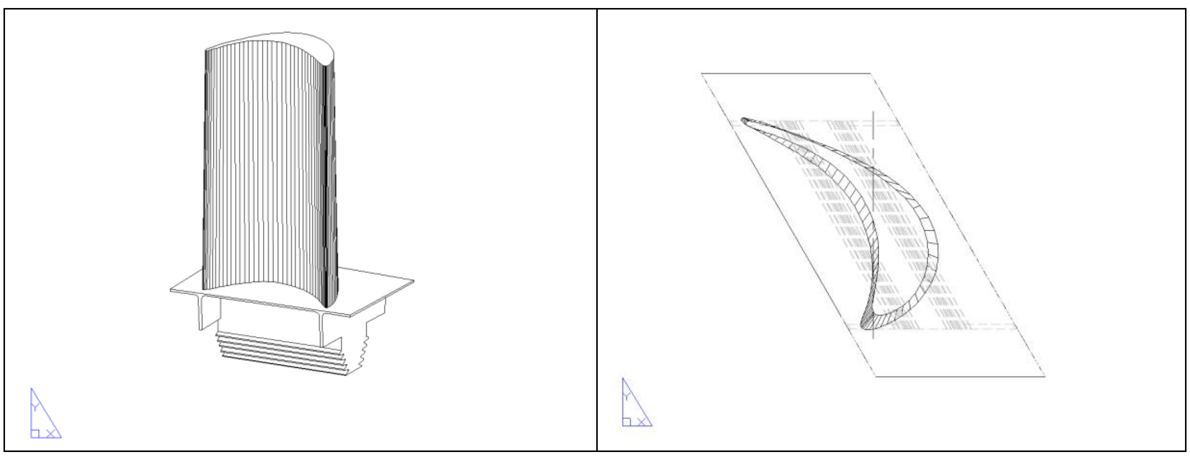

Figure 20. CAD design of rotor blade and root for mechanical analysis.

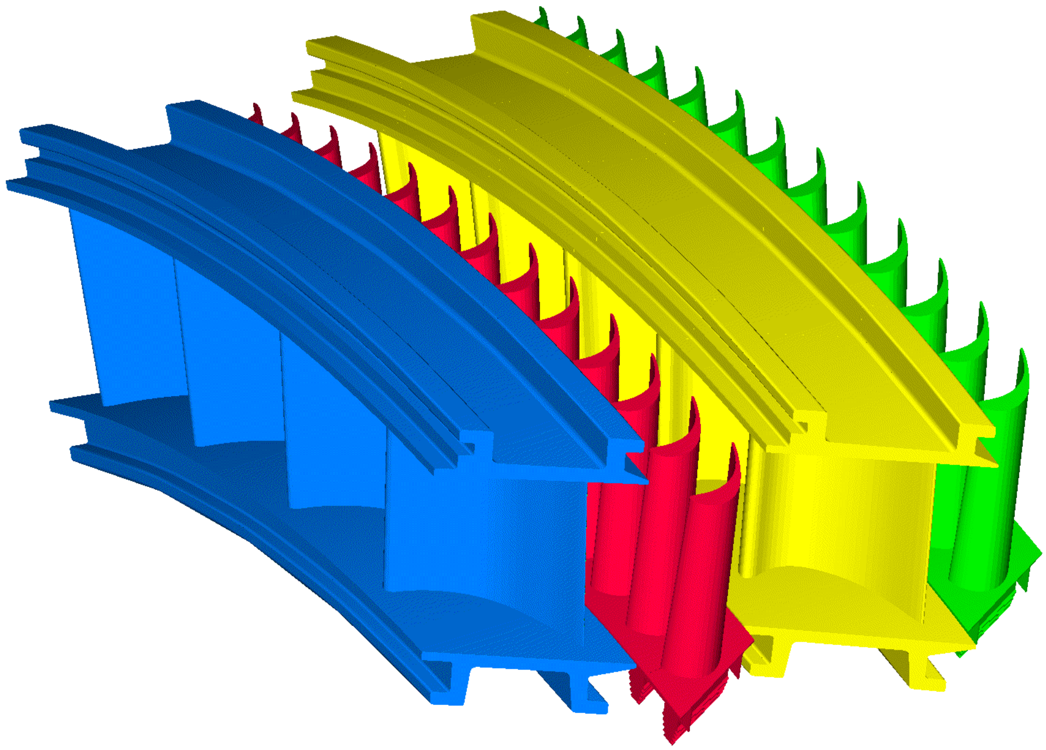

Figure 21. CAD design of the first and second HPT stages.

HTR-E WP1
-
PART II - HELIUM COMPRESSOR DESIGN

1. Design Conditions.

The design conditions for the LP and HP compressors are shown in Table 1.

	LPC	HPC
Working Gas	Helium	
Type	Horizontal axial flow	
Rotational Speed	3000 RPM	
Mass Flow Rate	317.5 kg/s	
Inlet Temperature	299 K	301 K
Inlet Pressure	25.5 bar	42.8 bar
Outlet Pressure	43.4 bar	79.6 bar
Pressure Ratio	1.702	1.860

Table 1. Design conditions for the LP and HP compressors.

2. Helium properties.

The main properties of the helium necessary for the design are presented in Table 1. The data were gathered from the Gas Encyclopaedia (1976), Bammert, (1969) and Muga (2002).

Cp [J / kg K]	5196
R [J / kg K]	2078
γ [-]	1.666
Speed of sound [m/s] at 952 K	1815.6

Table 1. Helium data.

The viscosity in Pa∗s is plotted in Figure 1 as a function of temperature. Based on data published in the Handbook of Chemistry (Lide, 1993) a power law was derived. Note that the viscosity of He is almost independent of the pressure level; from 1 to 100 bar the maximum variation in viscosity is 0.46% of the value given at 10 bar. Data presented in Figure 1 are the values at 10 bar and used in all the calculations.

The choice of Helium as a working fluid affects the turbo-machinery preliminary design in two ways :

1. - The number of compressor stages needed to obtain the required pressure ratio and high efficiency

2. - The machine size for a high pressure closed system.

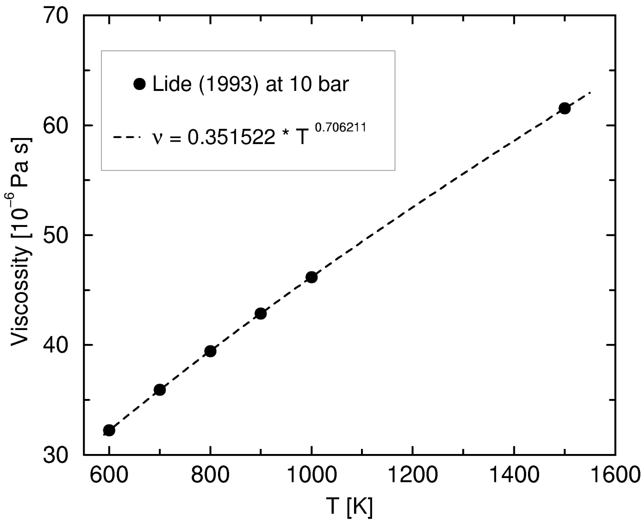

Figure 1. Viscosity of Helium as a function of the temperature.

The specific heat of helium is five times that of air, and since the stage temperature rise varies inversely with the specific heat (for a given limiting blade speed), it follows that the temperature rise available per stage when running with helium will be only one-fifth that of air.

The pressure ratio is given by Equation 2 :

$$\Pi = 1 + \left(\frac{\eta \cdot \Delta T}{T_1}\right)^{\frac{\gamma}{\gamma - 1}} \tag{2.2}$$

It can be seen that the combination of the temperature rise and the reduced value of γ/γ-1 results into a higher number of stages required for a Helium compressor.
As discussed previously, it is fortunate that the optimization (for maximum cycle efficiency) of a highly recuperated closed-cycle system gives a relatively low-pressure ratio; hence the number of compressor stages is comparable with existing open-cycle industrial gas turbines.

On the other hand, substitution of helium for air greatly modifies aerodynamic requirements by removing Mach number limitations.

The size of the machine is dictated by the choice of peripheral blade speed, there being an incentive to use the highest values possible commensurate with stress limits to reduce the number of stages since the stage-loading factor is inversely proportional to the blade speed squared.

For the preliminary design and to have the best efficiency following first-design conditions were employed:
1) Solidity at mid-span (chord length/pitch) = 1.2
2) Aspect ratio (blade height/chord length) = 1.5 – 2
3) As a first guess the annulus will be designed with constant hub and tip radius

4) Hub to Tip ratio (R_{hub}/R_{tip}) around 0.9
5) After each stage the flow will come out totally axial.

Initially a 16-stage LP compressor and a 24-stage HP compressor design was selected with both aerodynamic and dynamic loading parameters consistent with conservative design for long life industrial gas turbines.

3. Existing Helium turbine projects.

Based on a bibliography research it was concluded that currently there are in the world six different projects of high temperature reactors with a direct closed cycle of Helium, namely:

- PBMR: Pebble bed modular reactor (South Africa)
- HTGR: High Temperature Gas cooled Reactor (Japan)
- HTR-10: High Temperature Reactor (China)
- ACACIA: (Holland)
- GT-MHR:(Russia)

		GT-MHR	HTGR	HTR-10	ACACIA	PBMR		
						HP	LP	Power
	RPM	3000	3600	3000	3000	9000	8500	3000
	m [kg/s]	316.0	438.0	4.3	25.0	133.0	133.0	133.0
Turbine	Tinlet [K]	1121.2	1123.2	973.2	1073.2	1173.2	1076.2	952.2
	Toutlet [K]	783.2	891.7	525.6	765.0	1076.2	952.2	769.2
	Pinlet [bar]	70.1	68.4	30.0	23.0	90.0	72.0	53.0
	Poutlet [bar]	26.4	36.6			72.0	53.0	29.0
Compressor	Tinlet [K]	299.9				305.2	305.2	
	Toutlet [K]	382.1				375.2	408.2	
Power [MW]	compressor	269.8				48.4	71.2	
	turbine	555.0	526.7	10.0	40.0	67.0	85.7	126.5
	generator	285.2						126.5

Table 3. Cycle characteristics of the helium direct turbo-reactors.

Table 3 summarizes the main cycle characteristics from the different power plants. The data was collected from different sources: Muga (2002), Ballot (2002), Kemp (2002).

The GT-MHR delivers an electrical power of about 300 MW. In a similar way to the Japanese project, the turbomachine is arranged in a single shaft. However the HTGR-GT is rotating at 3600 RPM and the turbo-generator has a horizontal layout, whereas the GT-MHR (Figure 2) rotates at 3000 RPM and the turbo-generator is placed in vertical position.

There is much less known about the compressor than for the turbine and a complete new design must be made to optimize the geometry. The input for the LP and HP compressor design has been based on the reports of Romantsov (2002) and Muto et al.(1999). The Russian design indicates 16 and 24 stages for respectively the LP and HP compressor.

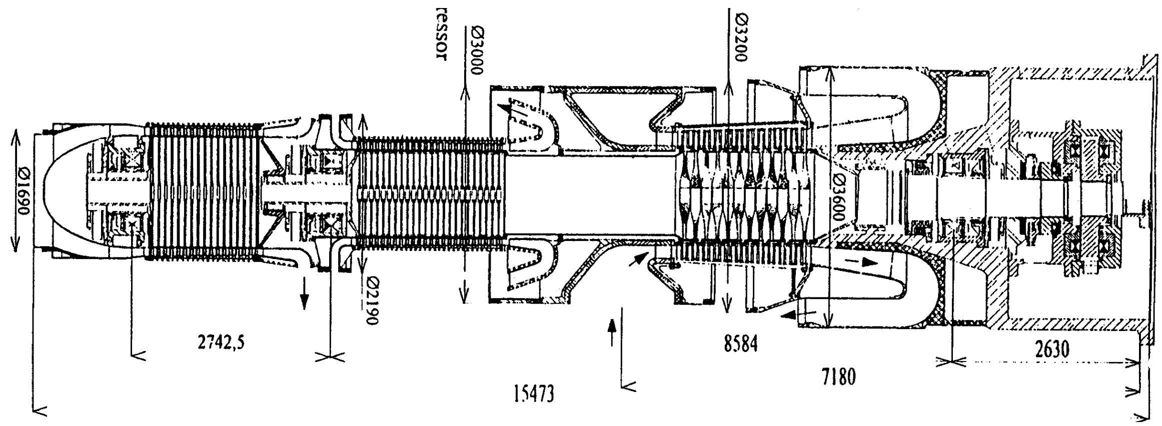

Figure 2. Sketch of the turbo-compressor for the GT-MHR, Perez Muga (2002).

The Japanese article provides more information about the compressor geometry but operating at 3600 RPM. The main characteristics of this design are reproduced in Figure 3 and Table 4 below. Some important points of the Japanese design are the number of stages : 16 LPC stages and 17 HPC stages at 3600 RPM with constant inner and outer casing diameters.

Table 4 Results of compressor design

Items	LPC	HPC
Outer diameter (m)	1.752	1.628
Inner diameter (m)	1.532	1.498
Hub to tip ratio	0.874	0.92
Blade height (m)	0.110	0.065
Rotor length (m)	2.10	1.32
Axial inlet gas velocity (m/s)	186.6	179.5
Axial exit gas velocity (m/s)	129.9	124.6
Adiabatic efficiency (%)	90.14	89.96
Politropic efficiency (%)	91.25	91.25
Exhaust section length (m)	0.338	0.192
Exhaust section inlet to outlet area ratio	1.523	1.488
Exhaust section pressure ratio	0.511	0.504
Pressure loss at the exhaust section (%)	0.491	0.457
Adiabatic efficiency including exhaust section (%)	89.33	89.21
Motive power (MW)	146.8	148.3
Thrust (t)	46.8	50.5
Number of blades per stage	112	181
Weight of one blade (kg)	0.2	0.041
Weight of one disc (in case of solid) (kg)	1400	764
Weight of one disc (in case of hollow) (kg)	1094	479

Table 4. Results of Japanese compressor design, Muto (1999).

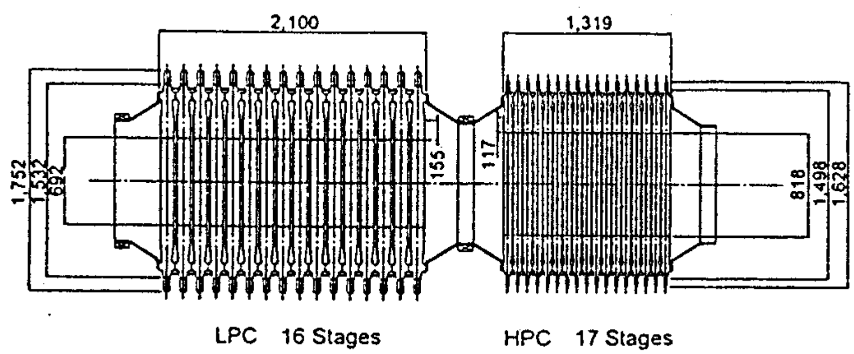

Figure 3. Sectional view of Japanese compressor rotor, Muto (1999).

4. Preliminary Design / Through-Flow Analysis.

a. Through-flow analysis program – ACD.

The computer code used for the aerodynamic design is a "Streamline Curvature" method. In this method the meridional plane (or "middle plane") is a longitudinal cross-section taken in the r-z plane. This plane is divided in the different stages for which the machine is being designed (Figure 4), plus some empty stations that are used to create data points for a spline fit of the streamlines. This is done in order to calculate the slopes and radii of curvature of the streamlines at their intersections points of each section face.

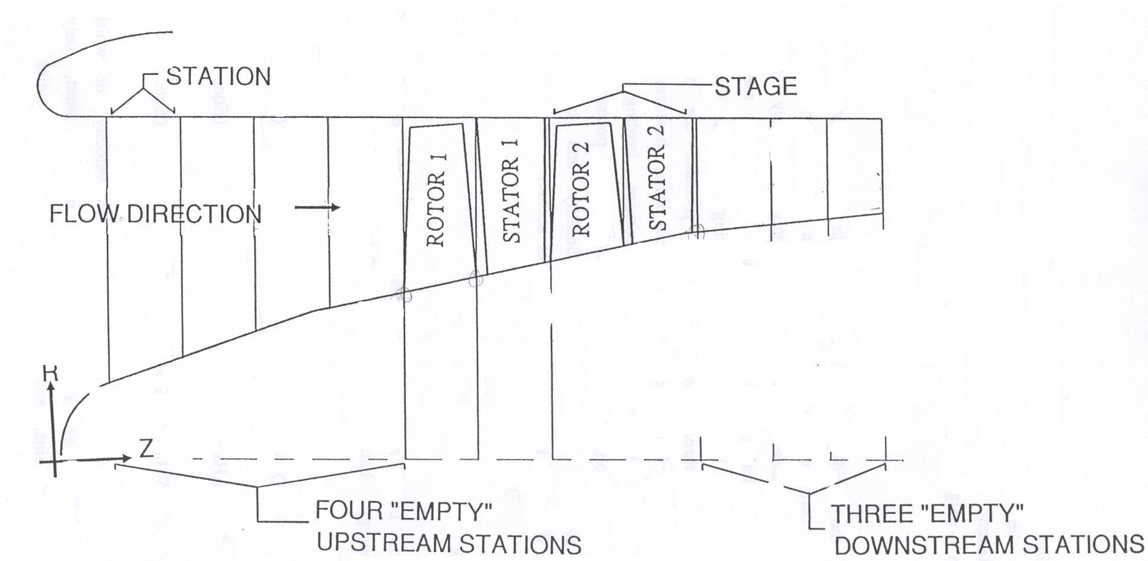

Figure 4. Meridional Plane Section for Trough-Flow Analysis.

The design program provides velocity diagrams on selected streamlines of revolution at the blade row edges. Steady axisymmetric flow is assumed and the aerodynamic solution is for the two-dimensional flow field in the meridional plane. The code obtains solutions to the equations of motion which neglect blade forces and are only valid for calculating stations outside blade rows. The streamline curvatures are computed from spline curve fits through calculated streamline locations for each station.

The input to the design code consists of the flowpath geometry including the axial location of blade row edges, overall total pressure ratio, mass flow, and rotational speed.

The radial energy distribution is specified by mean of a non-dimensional total pressure distribution p0/p0,tip. Since the higher endwall blade losses generally result in higher energy addition in the rotor hub and tip regions, the imposed pressure profile was designed to slightly reduce the loading in those regions.

The maximum acceptable loading is then restricted by limits on the diffusion factor in critical regions like rotor tip and stator hub. A maximum tip tangential velocity can be imposed as well to limit the overall loading.

The choice of adequate solidities for each blade row finally determines the solution within the limits previously set.

b. ACD-2 Analysis.

The basis for the program analysis routines lies in the equations of continuity, energy balance and the Euler equation of fluid motion.

$$\dot{Q} = 2 \cdot \pi \cdot \int_{RHUB}^{RTIP} R \cdot \rho \cdot V_z \cdot dR \tag{3.1}$$

$$\Delta H_0 = \Delta \left[C_p \cdot T_{TOT} \right] \tag{3.2}$$

$$\Delta H_0 - T \Delta S = \vec{V} x rot \vec{V} \tag{3.3}$$

As the flow is axisymmetric and the tangential velocity or whirl distribution is defined as a function radius in the input, only the R component remains, and the number of usable equation is reduced fro 3 to 1.

$$(\Delta H_0 - T \Delta S = \vec{V} x rot \vec{V})_R \tag{3.4}$$

where H_0 is the enthalpy, T is the static temperature and V is the velocity vector.

$$\Delta H_0 = \Delta \left[C_p \cdot T_{TOT} \right] = \omega \cdot R \cdot \Delta V_\theta \tag{3.5}$$

Here, w is the angular velocity, C_p is the constant pressure specific heat, and V is the tangential velocity.
Using again the isentropic efficiency (equation 2.1), a relationship between the total pressure ratio, and temperature ratios.
Further a relationship between static pressure and temperatures, and fluid density is given by the ideal gas law

$$p = \rho R T \tag{3.6}$$

And finally, using the equation 3.1 the continuity law, is given the mass flow trough the channel. The sketch of a stage analysis is shown in Figure 5.

The loss calculation is based on

- Liblein subsonic profile correlations for efficiency.
- Correlations for end-wall boundary layer blockage.

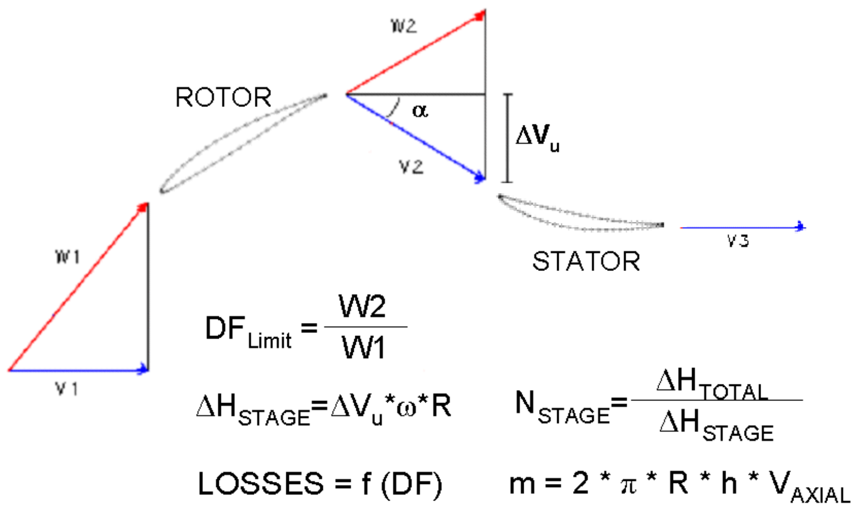

Figure 5. Multi-stage through-flow analysis.

c. Design parameters.

As it was imposed in the preliminary design, a constant radius design was first examined. But it came out as a result that there was a high decrease in the axial velocity. This high decrease had as result, that the velocity triangles from inlet to outlet were different.

So imposing a linear decrease in the blade height of 20% from inlet to outlet and imposing the same work in each stage allows to obtain an approximately constant axial velocity along from inlet to outlet. The inlet and outlet flow angles are almost identical in each stage, which allows to design only a single (intermediate) stage in terms of blade shape for each compressor (except for the first and last stages).

In the axial stages the limit imposed for the maximum diffusion factor (aerodynamic loading factor) is of the order of 0.39. In the LPC results, came out a diffusion factor between 0.39 and 0.375 in all stages, which is a rather conservative value for high targeted efficiency. In the HPC, the diffusion factor was limited to 0.35 at the rotor tip and 0.34 at the stator hub. These low values were imposed because of the small blade height.

4.4. Results of Preliminary Design.

4.4.1. LPC Results.

- Only 15 stages are needed to produce the required pressure ratio instead of the 16 stages predicted at the beginning mainly due to the contraction along the machine.

- Blade height varies from 0.084 m at inlet to 0.0685 at the last stage. As explained before this will allow a constant axial velocity from inlet to outlet.
- The predicted (total-to-total) efficiency for the full scale LP compressor is 88.5%, not taking into account the tip clearance and inlet and outlet duct losses.

4.4.2. HPC Results.

- The program predicts that only 21 stages are required instead of 24 as in our initial guess, again due to the decreasing annulus area from inlet to outlet.
- Average radius is approximately 0.743 m. at the inlet and 0.738 m. at the outlet
- Blade height varies from 0.0548 m. at inlet to 0.047 m. at the last stage. This allows again a constant axial velocity from inlet to outlet.
- The predicted (total-to-total) efficiency for the full scale LP compressor is 87.4%.

5. Design Optimization.

A disadvantage of this type of design is that it results in relatively small blade heights mostly for the HP compressor. The LP blades vary between 8.4 cm and 6.85 cm height. The HP blades vary between 5.48 cm and 4.7 cm height. Low aspect ratio blades are of course subject to higher secondary losses and efficiency can be improved by increasing the blade height.

The degree of reaction of this first design is around 0.8, which is a result from the initial choice to have axial outlet flow at the exit of each stage. This is actually a constraint that can be taken out, at least for the intermediate stages. Of course the last stage will have to produce a nearly zero exit swirl.

According to Vravra (Figure 6), it can be shown that the best efficiency is obtained for a 0.5 degree of reaction and a 0.5 flow factor. The optimization of the first design was therefore performed in order to reduce the flow factor from 0.75 in the initial design to about 0.5 and to reduce the degree of reaction from 0.8 to 0.5 as well (Figure 7).

The reduction of the flow factor will lead to increased blade heights which is not only better for the reduction of secondary flow effects but also for the reduction of tip clearance losses. Tip clearance losses are one of the key points in the design of a single-shaft machine as the present one, since the length of the shaft makes it very difficult to achieve a good control of the tip clearance during operation.

Tip clearance losses cause very detrimental effects to the performance of the compressor and experimental tests have shown that a 1 % increase of the relative tip clearance gap δ/H results into a loss of 2 % of the efficiency!

$$\Delta\eta_{\text{tip clearance losses}} = -2\,\delta/H$$

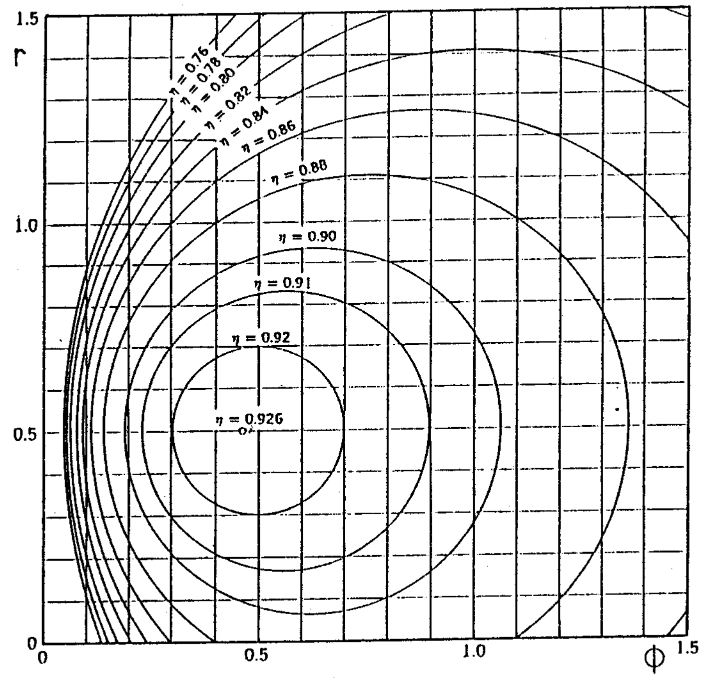

Figure 6. Variation of the efficiency of a compressor stage as a function of the degree of reaction and flow factor, Vavra.

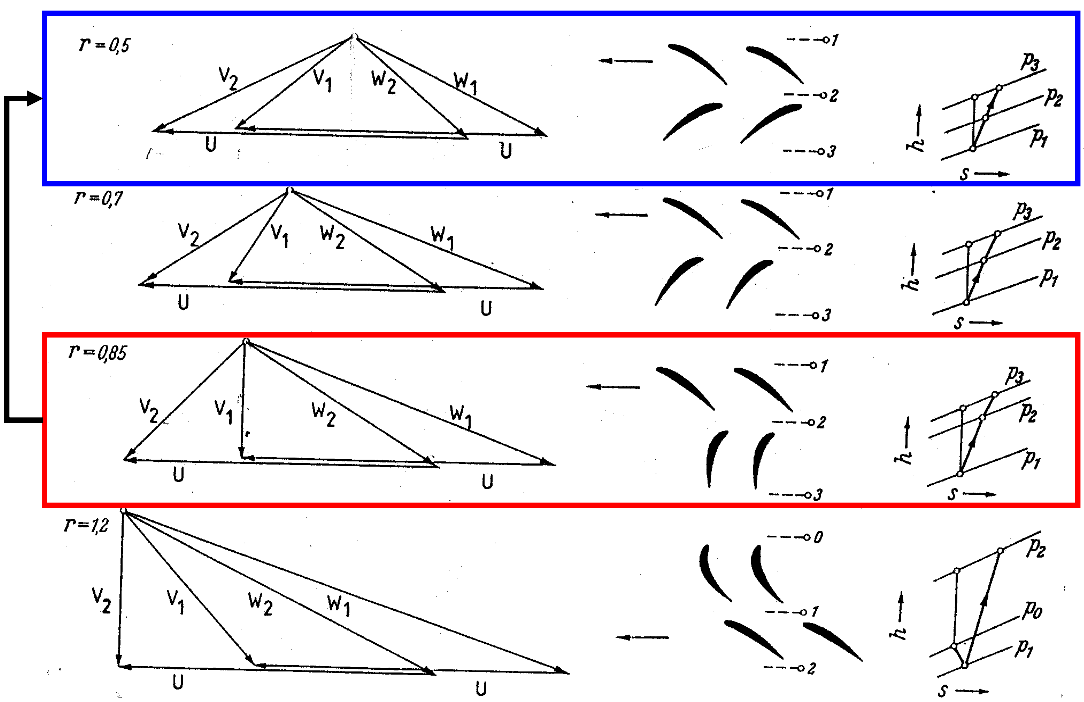

Figure 7. Degree of reaction in compressor stages.

The process of optimization can be followed in Figure 8, which features efficiency versus number of stages.

If we consider our first LPC configuration, we obtain the 3 points with circular symbols on the vertical line at the 15-stage abscissa. All 3 points correspond a flow factor of 0.75 as previously described. The highest point in efficiency corresponds to the total-to-total efficiency of this particular configuration (88.5%). With a flow factor of 0.75, the blades are smaller and the exit kinetic energy at the compressor outlet remains relatively high. The total-to-static efficiency (84%) therefore drops by a large amount compared to the total-to-total efficiency. Those efficiencies still do not take into account the tip clearance losses, which, for the corresponding blade height amount to –2.4%. We finally obtain a more realistic estimation of the efficiency of 81.7%.

Reducing the flow factor from 0.75 to 0.5 and reducing the degree of reaction for all intermediate stages from 0.8 to 0.5 leads us to a 20-stage configuration at the very right hand side of the graph. The achieved total-to-total efficiency (87%) is slightly lower since the increased number of stages leads to more friction losses which are only partially offset by the gain in blade height. Regarding the total-to-static efficiency, since the blade height has increased, the (lost) exit kinetic energy decreases and leads to a smaller drop from the total-to-total efficiency. We achieve 84.3% from which now only –1.75% tip clearance losses have to be substracted again due to the increased blade height to obtain 82.6%.

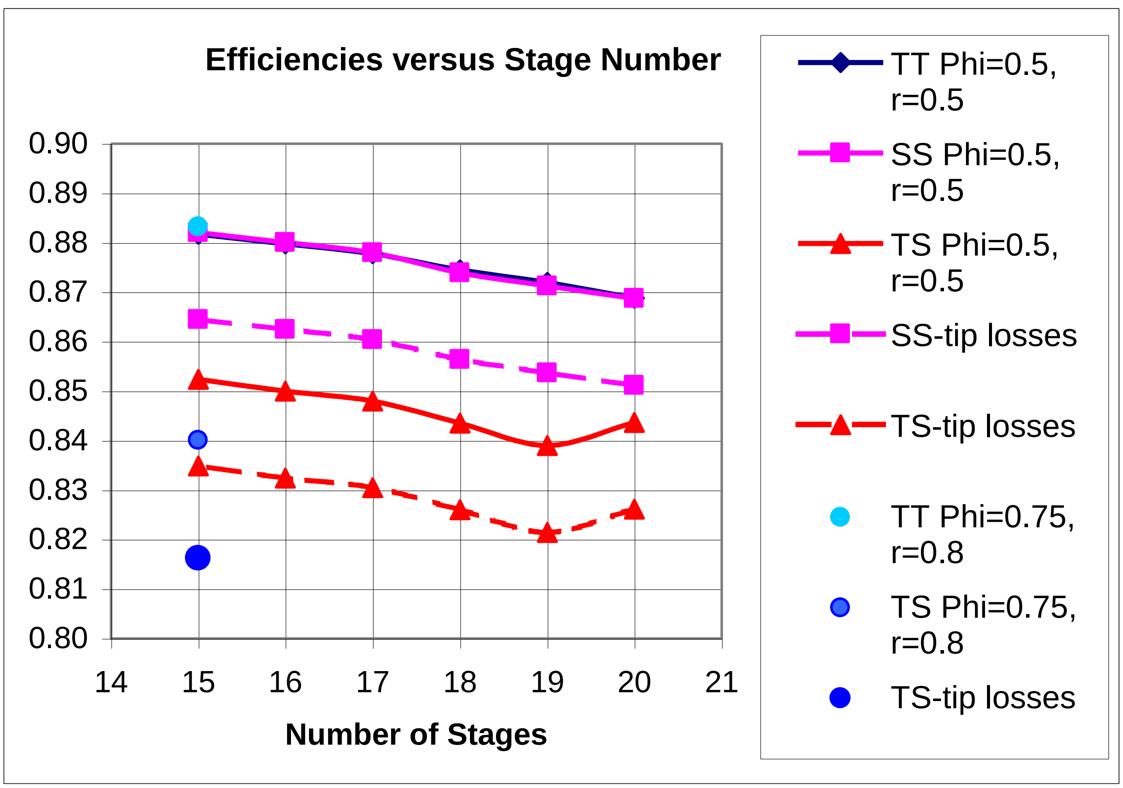

Figure 8. Optimization process illustrated in efficiency diagram versus stage count.

This new 20-stage configuration proves itself to be better already than the original one at least in terms of efficiency. Of course the number of stages is prohibitive, but both designs were based on very conservative values of diffusion factor. So there is still some room to increase the blade loading of each stage in order to reduce the stage count.

This is precisely what was done as we follow the bottom dotted line with triangular symbols. The limits of the diffusion factors in all rotating and non-rotating blade rows were increased (within the limits of acceptable losses and loadings) and the solidities were also slightly decreased because this helps diffusion. Lower solidities means lower blade count and in turn results in lower friction losses.

This allows to get back highlight several new solutions starting from a 17-stage configuration with an efficiency of 83%, a 16-stage configuration with an efficiency of 83.2% or a 15-stage configuration with an efficiency of 83.5%. The latter shows a 1.8% higher efficiency than our original solution with the same number of stages. This configuration was therefore chosen for further development.

The same design philosophy was adopted to design the 18-stage HP compressor. All the aerodynamic details of both configurations are listed in Table 5.

	LPC	HPC
Number of Stages	**15**	**18**
Flow Coefficient Phi [-]	0.51	0.56
Degree of Reaction	0.48	0.5
Stator exit swirl velocity [m/s]	85	75
Turning Rotor 7 (hub-tip)	30.0-20.0	28.5-23.6
Turning Stator 7 (hub-tip)	22.7-22.5	25.4-24.8
Diffusion Factor Rotor 7 (hub-tip)	0.55-0.56	0.54-0.56
Diffusion Factor Stator 7 (hub-tip)	0.55-0.55	0.54-0.56
Average TT Efficiency Rotor 7	0.9539	0.9524
Solidity Rotor 7 (hub-tip)	1.11-0.99	1.11-0.99
Average TT Efficiency Stage 7	0.8929	0.8942
Solidity Stator 7 (hub-tip)	1.099-0.98	1.099-0.98
Tip Radius First Rotor [m]	0.9	0.85
Aspect Ratio [-]	0.8733	0.9235
Blade Height [cm]	11.4	6.5
Rotor Length [m]	1.965	1.3968
Inlet Static Pressure [bar]	25.10	42.08
Inlet Static Temperature [K]	297.14	298.99
Outlet Static Pressure [bar]	42.70	78.99
Outlet Static Temperature [K]	376.91	396.18
OSPR	1.7012	1.8773
Outlet Total Pressure [bar]	43.39	80.20
OPR	**1.7014**	**1.8739**
Outlet Total Temperature [K]	379.33	398.60
OTR	1.27	1.32
Power [MW]	**132.52**	**164.31**
Average Work per Stage	27469.77	28040.68
TT Efficiency [-]	0.8817	0.8807
SS Efficiency [-]	0.8820	0.8814
TS Efficiency [-]	0.8524	0.8567
Clearance [delta/H] for 1 mm	0.0088	0.0154
Tip Clearance Efficiency Loss	0.0175	0.0308
SS Efficiency - Tip Cl. Losses	0.8645	0.8507
TS Efficiency - Tip Cl. Losses	0.8349	0.8259

Table 5. Aerodynamic design results for the design of the LPC and HPC.

6. <u>Blade Design.</u>

The two-dimensional design of the blade sections is done by means of an inverse design and optimization method. The latter uses an iterative approach that combines a direct solver with a blade geometry modification algorithm. A potential flow method was used in the present blade design. The procedure starts with the analysis of a given cascade geometry using the flow solver. The differences between the calculated and required velocity is used as an input for the modification algorithm based on a transpiration technique. This algorithm provides a new blade shape for which the calculated velocity distribution is closer to the desired one. A major advantage of this method is that the design cycle is very short and allows an easy off-design analysis since the same code is used for the blade design and the analysis for different inlet flow conditions.

The design cycle is represented in the Figure 9, the procedure being started by the analysis of a NACA blade, for example. The definition of the initial geometry is based on the choice of appropriate values for the following parameters :

- Stagger angle
- Camber angle
- Thickness distribution

The solidity (or pitch-to-chord ratio) and the aerodynamic inlet flow angle are the outputs of the through-flow calculations. The velocity distribution is then modified to obtain a so-called controlled diffusion blade (Figure 10).

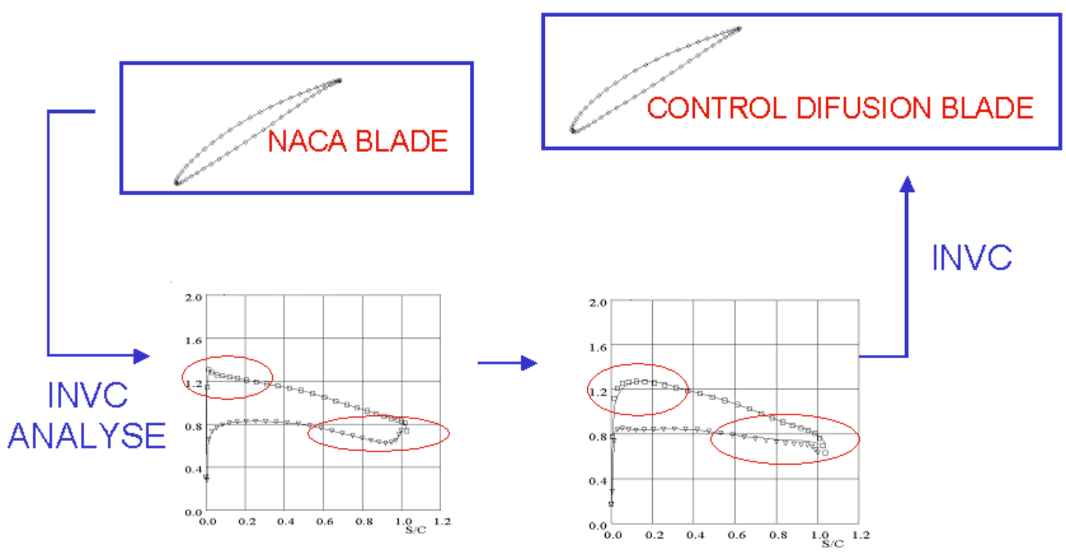

Figure 9. Inverse design procedure for compressor blades.

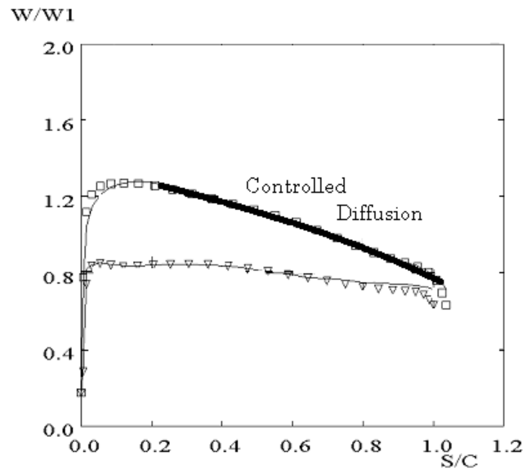

Figure 10. Velocity distribution on a controlled diffusion blade.

The two-dimensional blade design results are presented in Figures 11, 12, 13 and 14 respectively for an intermediate stage rotor and stator blade, respectively for the LPC and HPC.

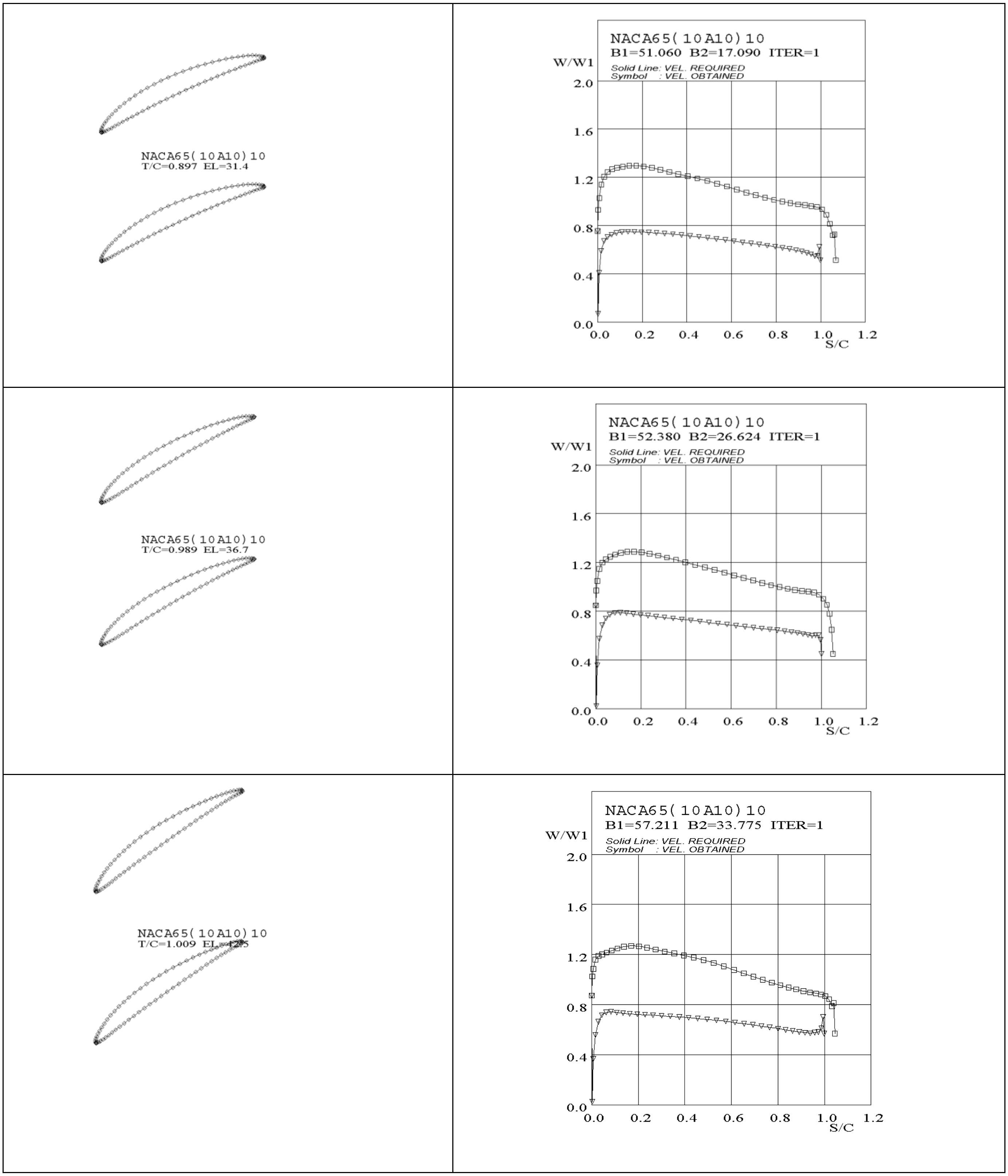

Figure 11. LPC Stage 7 rotor blade profiles and velocity distributions (hub/mid/tip).

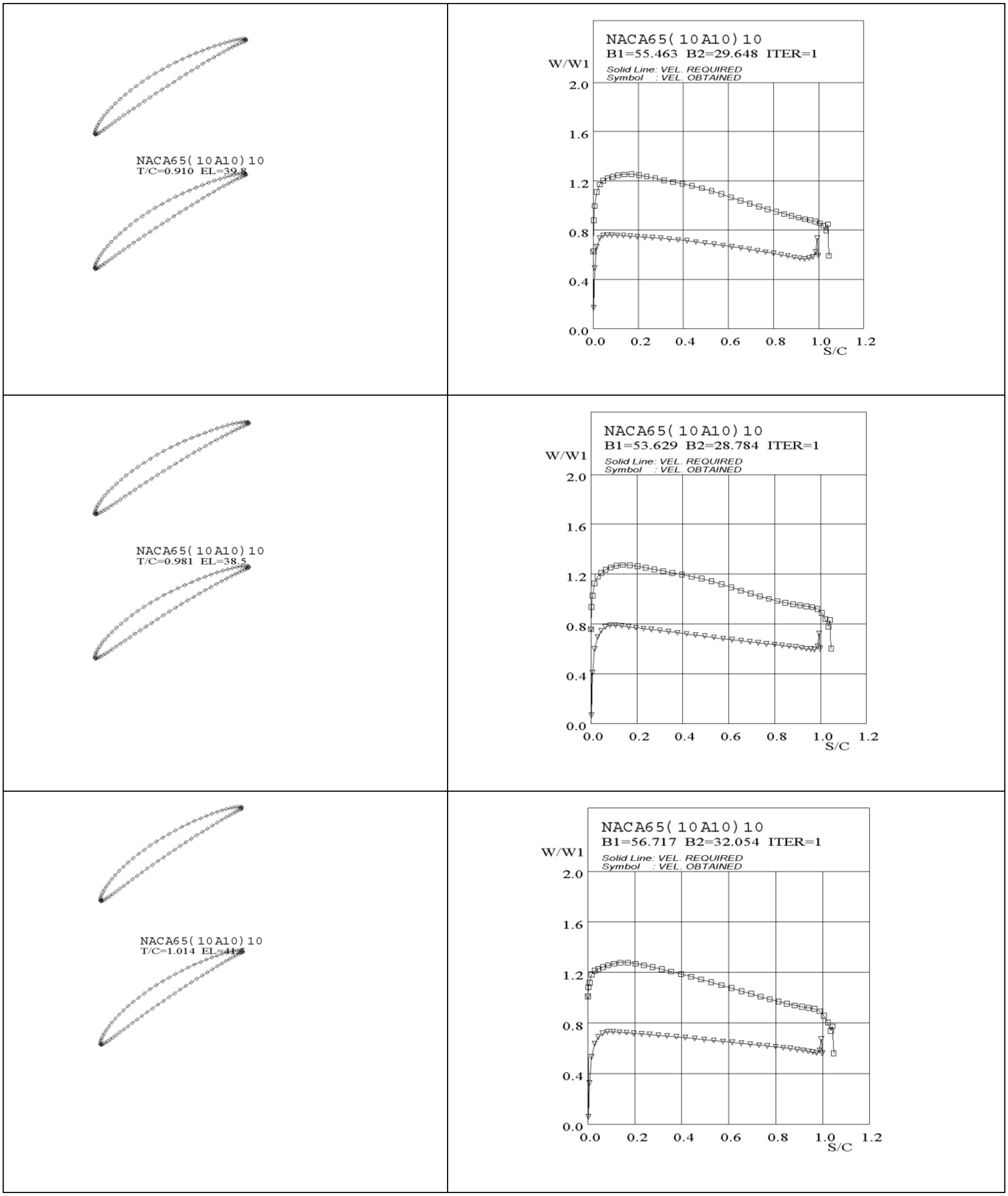

Figure 12. LPC Stage 7 stator blade profiles and velocity distributions (hub/mid/tip).

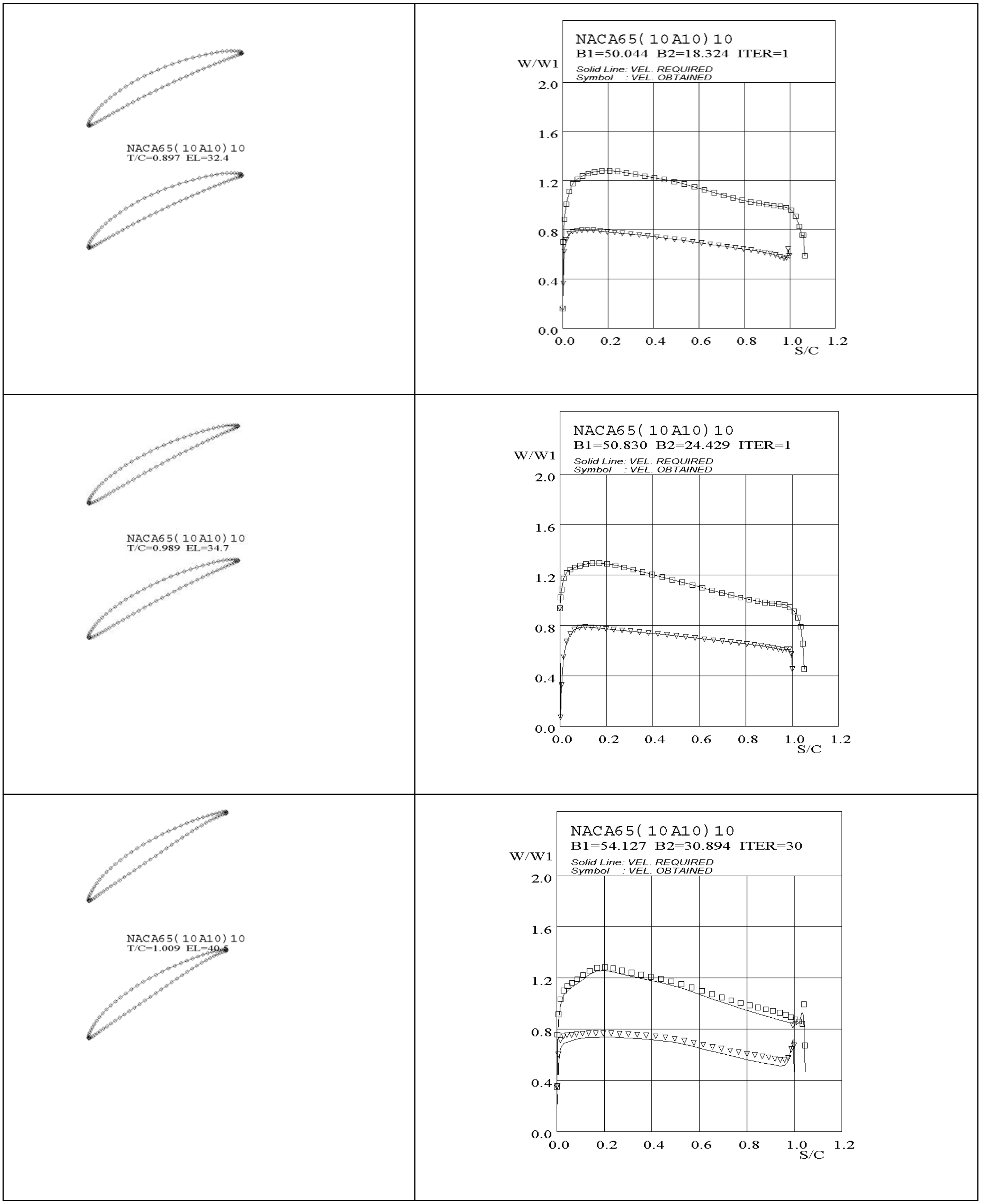

Figure 13. HPC Stage 7 rotor blade profiles and velocity distributions (hub/mid/tip).

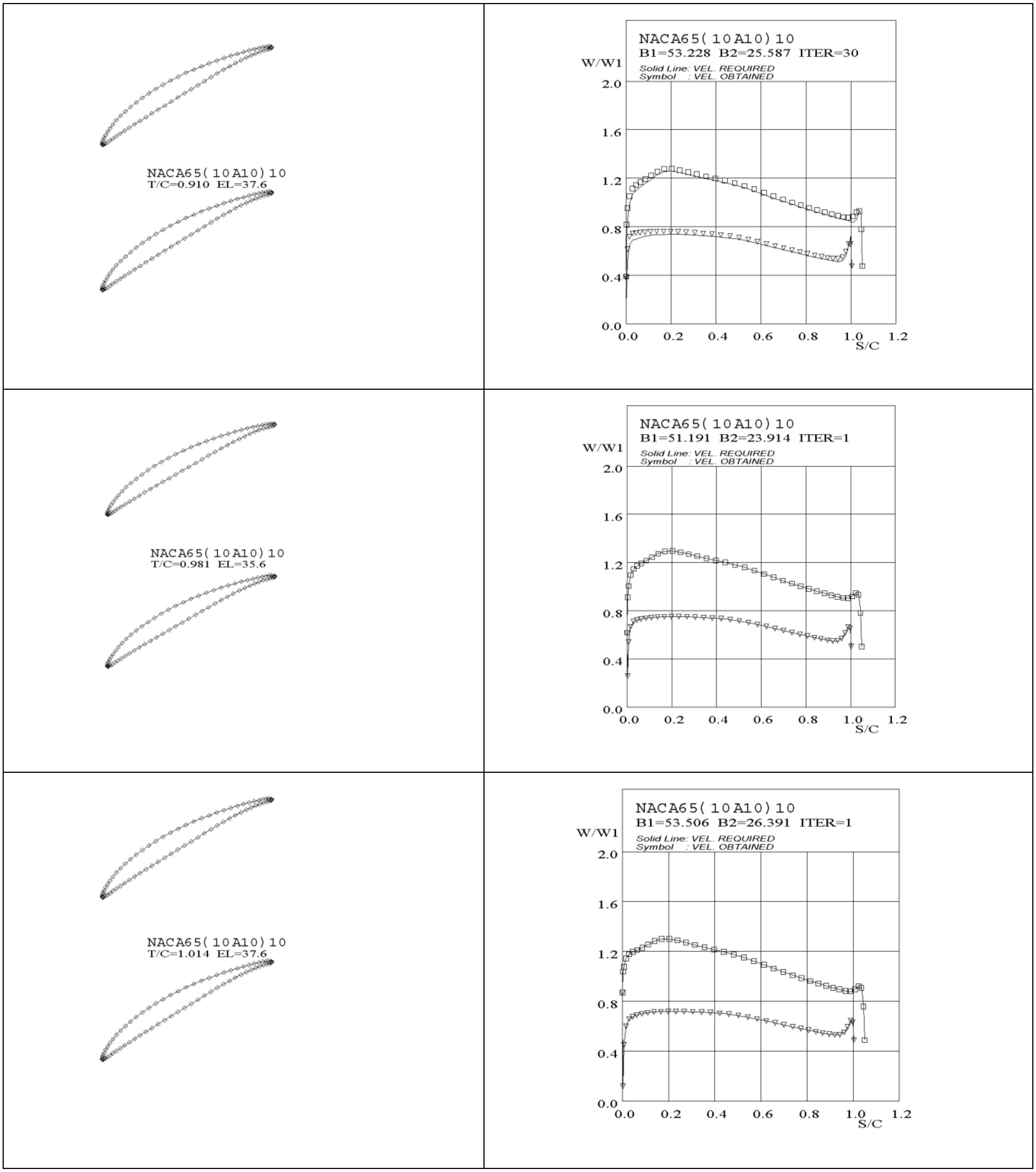

Figure 14. HPC Stage 7 stator blade profiles and velocity distributions (hub/mid/tip).

7. <u>Three-dimensional Navier-Stokes analysis.</u>

Since the two-dimensional blade design is performed with an inviscid method, the blade rows need to be analyzed by means of a Navier-Stokes solver to assess its viscous performance with respect to the one-dimensional through flow design.

Figure 15 and 16 show respectively the 3D blade stacking of the LPC and HPC rotor along the center of gravity of each section and for the stator, stacked along the leading edge. Figure 17 shows a top view of the intermediate stage with blade count as it has been designed and analyzed with the Navier-Stokes solver.

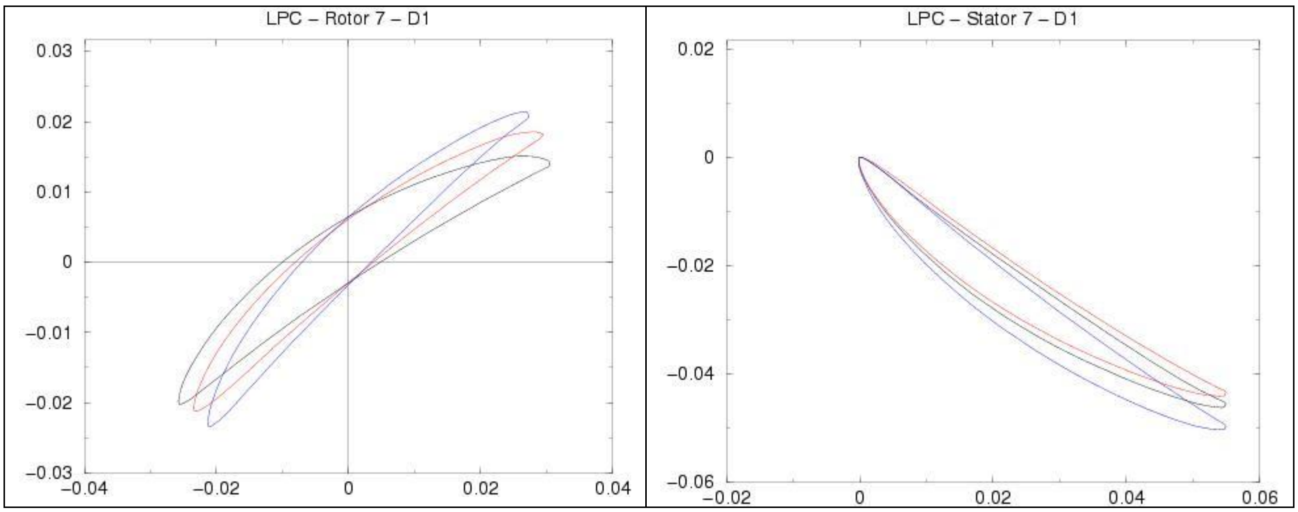

Figure 15. LPC rotor and stator 3D blade stacking.

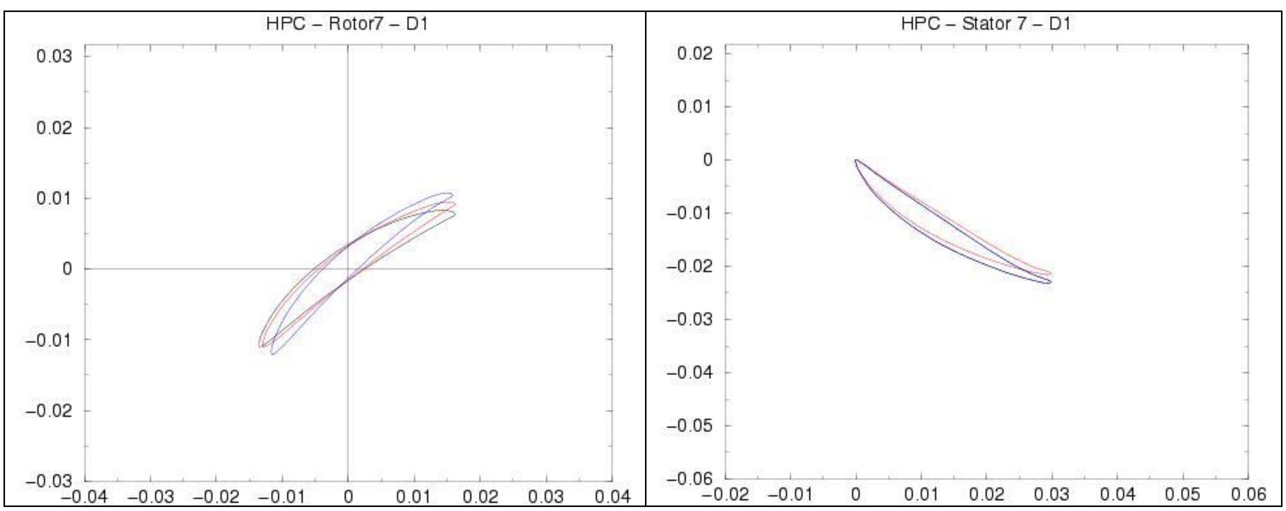

Figure 16. HPC rotor and stator 3D blade stacking.

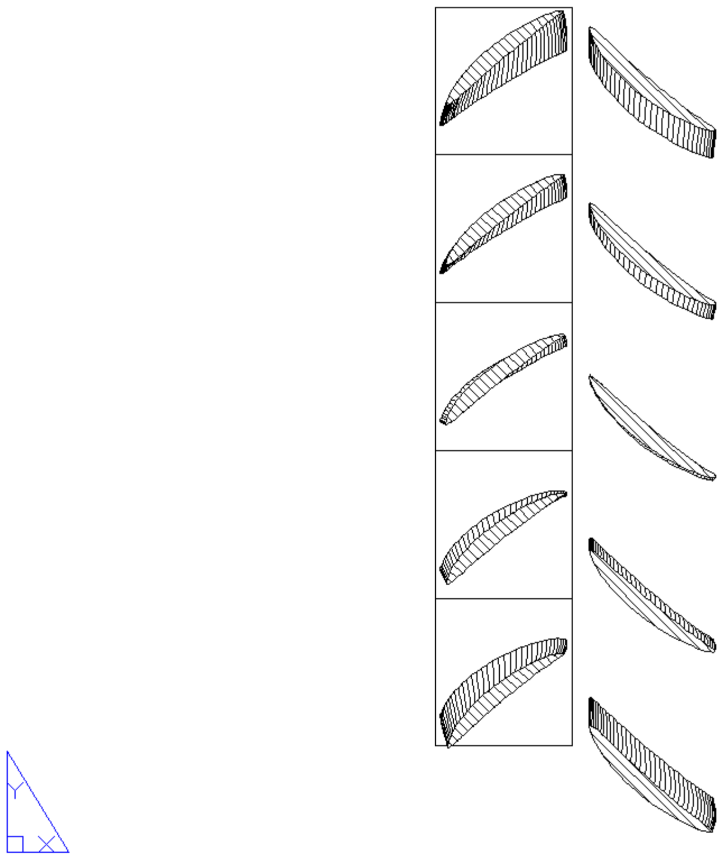

Figure 17. Top view of the LPC intermediate stage, 75 rotor blades, 69 stator blades.

The results of the Navier-Stokes computations are presented in the following figures.

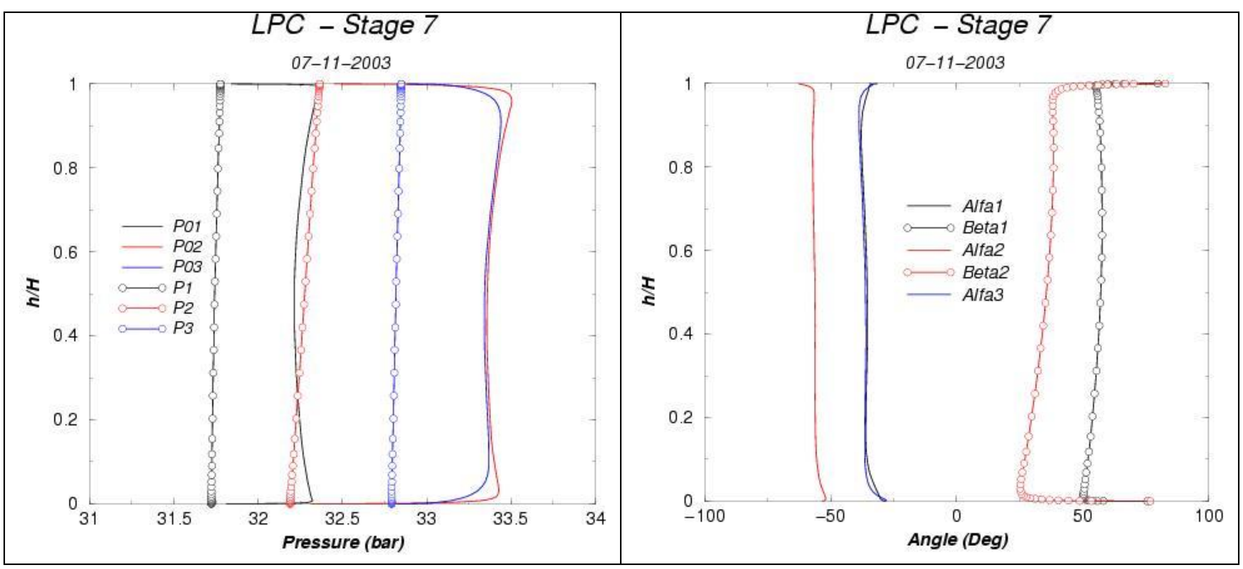

Figure 18. LPC Radial pressure and flow angle distributions.

Figure 18 shows the radial total and static pressure distributions as well as the flow angle distributions at the rotor inlet (1), rotor outlet (2) and stage outlet (3). Important to notice are the practically constant stage exit total pressure distribution (p03) and stage exit flow angle (alpha3) which is equal to the stage inlet flow angle (alpha1). This is particularly important for an intermediate stage.

The isentropic Mach number distributions are shown in Figure 19 for sthe LPC rotor and stator respectively at 10%, 50%, and 90% blade height. Both sets of distributions show a smooth deceleration as the blades have been designed for. The presence of a small velocity peak on rotor and stator at 50% span are due to incidence effects and need to be improved by modifying slightly the blade profiles at these locations.

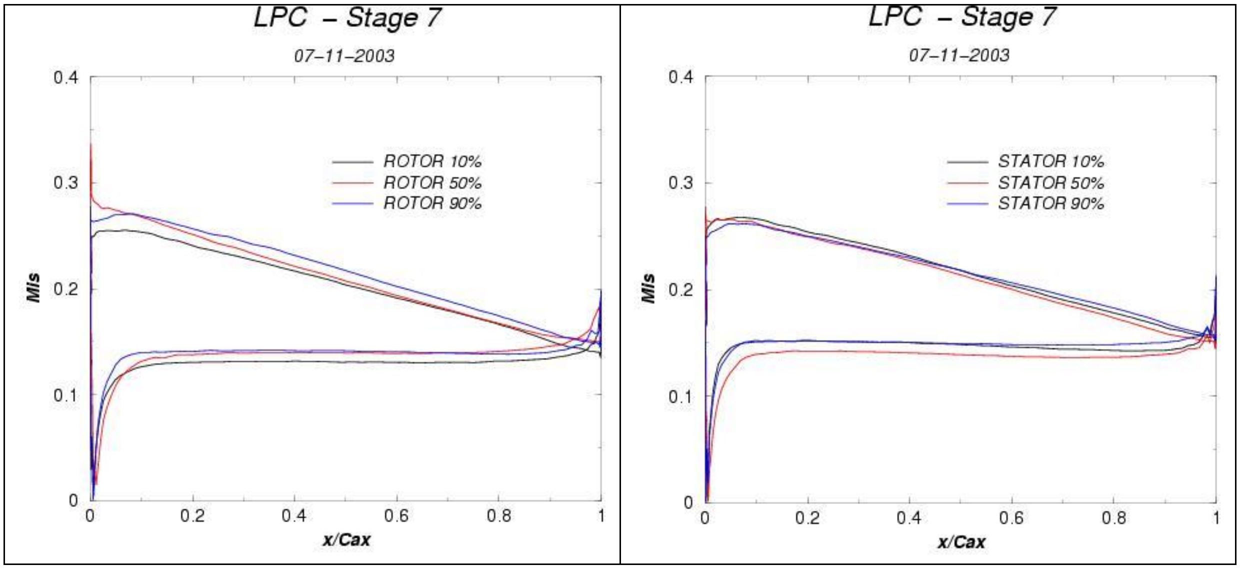

Figure 19. Isentropic Mach number distributions on LPC rotor and stator.

The same data are presented in Figure 20 and 21for the HPC intermediate stage and the same remarks apply.

Finally, Table 6 summarizes the obtained stage performance after the Navier-Stokes computations.

	LPC	HPC
Total-to-total stage eff. [-]	0.9480	0.9444
Total-to-total stage eff. [-]	0.9027	0.8958
Total-to-total stage eff. [-]	0.9470	0.9430
Stage Pressure Ratio [-]	1.0345	1.0351
Mass Flow Rate [kg/s]	313.54	310.98

Table 6. Performance characteristics obtained after Navier-Stokes computations for the LPC and HPC intermediate compressor stages.

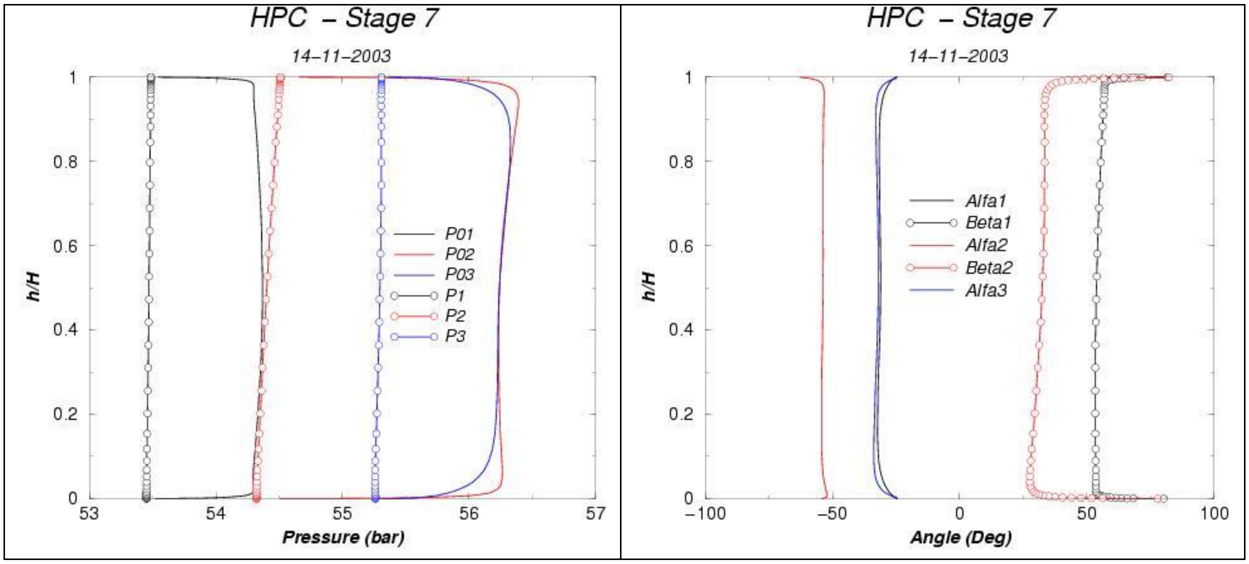

Figure 20. HPC Radial pressure and flow angle distributions.

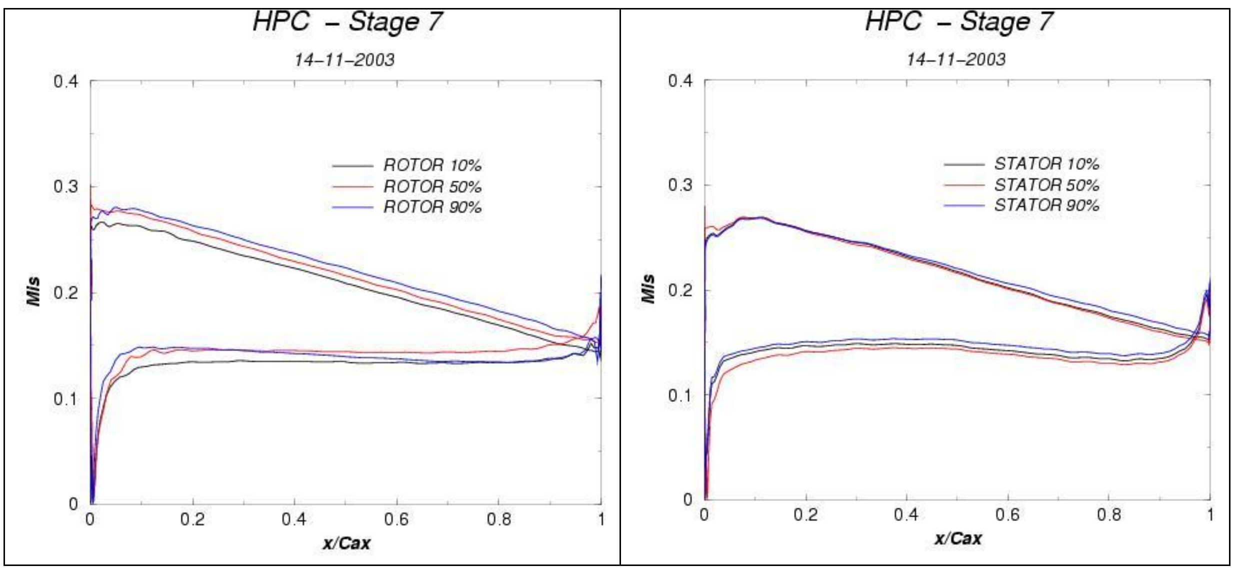

Figure 21. Isentropic Mach number distributions on HPC rotor and stator.

8. CAD Design for Mechanical Analysis.

A CAD design of the LPC stage was carried out in order to allow the geometry to be transmitted to the contract partner (Empresarios Agrupados) in charge of the mechanical analysis. The rotor root design is of conventional type and the stator is cantilevered.

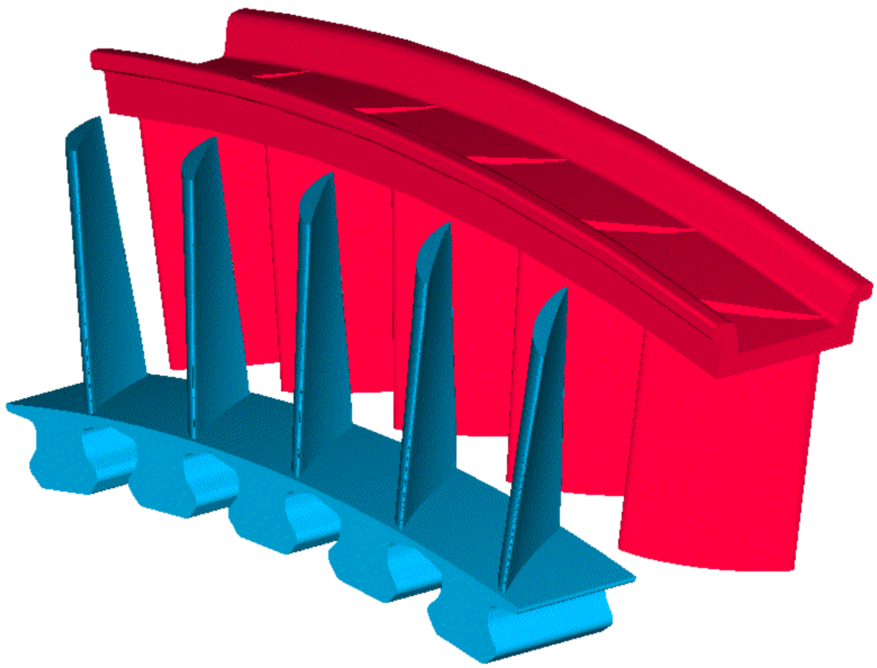

Figure 22. CAD design of the LPC intermediate stage.

9. Conclusions.

The complete aerodynamic design procedure of the helium turbomachine has been described in the present report according to the specifications of the direct helium cycle.

A review of existing technologies and know-how from past HTR experience has been performed. The Russian GTMHR and Japanese HTGR projects mainly habe been used for comparison with the current design.

At this stage, the aerodynamic design results in the following layout : a 12-stage turbine with a 15-stage LPC and an 18-stage HPC. This configuration results from an optimization process on many aerodynamic parameters, with the aim of keeping the smallest number of stages with the highest achievable efficiency. This optimization has been done on the basis of the Smith efficiency diagram for the turbine and on the Vavra efficiency diagram for the compressors.

Regarding the turbine, two full stages have been designed, i.e. the first and second turbine stages. The turbine has been designed in such a way that the second stage corresponds to any intermediate stage of the turbine, i.e. with the same blade geometry. Due to the area divergence along the turbine, only the blade count has to be slightly adjusted along the machine. The 2D blade design has been performed by means of an inverse design method and the full 3D geometry has been designed by means of a CAD program which has been sent to the partner in charge of the mechanical analysis (Empresarios Agrupados).

The performance of both turbine stages has been analyzed by means of Navier-Stokes computations and the results are in good agreement with the predicted performance by the one-dimensional design, i.e. a 93% total-to-total efficiency.

Regarding the LP and HP compressors, a typical intermediate stage has been fully designed and analyzed for each of them. The philosophy is very similar : the stage geometry can be repeated for all intermediate stages with an appropriate adjustment of the number of blades along the machine. Both intermediate LP and HP stages have been analyzed by Navier-Stokes computations as well showing respectively total-to-total efficiencies of 94.8% and 94.3%.

Those efficiency levels show the feasibility to design a helium turbomachine with good efficiency levels strictly from the aerodynamic point of view. Still, those efficiency values are not final since they do not include the inlet and outlet duct losses nor the tip clearance losses which are a very important point, not only from an aerodynamic point of view but also from a mechanical point of view. Mechanically, the smallest technologically possible tip clearance value should be communicated in order to calculate the efficiency drop related to it. It must be known that a 1 % increase in the relative tip clearance will result into a 2% relative decrease in efficiency.

Regarding the number of stages for the compressors, one stage could be added or substracted according to the use or not of a tandem stator for the exit stages and an IGV for the inlet stages will also favor off-design operation. Again recommendations about the shaft maximum total length would be welcome.

Finally, the result of the stress calculations could have a dramatic impact on the machine layout if the rotor diameter has to be decreased. This will inevitably lead to an increase of the number of stages. In a similar way, if disk cooling has to be applied, the complete cycle efficiency has to be recalculated and the performance of the machine as well due to the decrease of working massflow.

The future developments will lie in the investigations of efficiency gains by 3D blade shaping, shrouded turbine rotors or shrouded compressor stators.